Geological Society of America
Special Paper 403
2006

U-Pb SHRIMP geochronology and trace-element geochemistry of coesite-bearing zircons, North-East Greenland Caledonides

William C. McClelland*
Department of Geological Sciences, University of Idaho, Moscow, Idaho 83844, USA
Siobhán E. Power
Jane A. Gilotti
Department of Geoscience, University of Iowa, Iowa City, Iowa 52242, USA
Frank K. Mazdab
U.S Geological Survey–Stanford Ion Probe Laboratory, 367 Panama Mall, Stanford, California 94305, USA
Brigitte Wopenka
Department of Earth and Planetary Sciences, Washington University, St. Louis, Missouri 63130, USA

ABSTRACT

Obtaining reliable estimates for the timing of eclogite-facies metamorphism is critical to establishing models for the formation and exhumation of high-pressure and ultrahigh-pressure (UHP) metamorphic terranes in collisional orogens. The presence of pressure-dependent phases, such as coesite, included in metamorphic zircon is generally regarded as evidence that zircon growth occurred at UHP conditions and, if dated, should provide the necessary timing information. We report U-Pb sensitive high-resolution ion microprobe (SHRIMP) ages and trace-element SHRIMP data from coesite-bearing zircon suites formed during UHP metamorphism in the North-East Greenland Caledonides. Kyanite eclogite and quartzofeldspathic host gneiss samples from an island in Jøkelbugt (78°00′N, 18°04′W) contained subspherical zircons with well-defined domains in cathodoluminescence (CL) images. The presence of coesite is confirmed by Raman spectroscopy in six zircons from four samples. Additional components of the eclogite-facies inclusion suite include kyanite, omphacite, garnet, and rutile. The trace-element signatures in core domains reflect modification of igneous protolith zircon. Rim signatures show flat heavy rare earth element (HREE) patterns that are characteristic of eclogite-facies zircon. The kyanite eclogites generally lack a Eu anomaly, whereas a negative Eu anomaly persists in all domains of the host gneiss. The ^{207}Pb-corrected ^{206}Pb/^{238}U ages range from 330 to 390 Ma for the host gneiss and 330–370 Ma for the kyanite eclogite. Weighted mean ^{206}Pb/^{238}U ages for coesite-bearing domains vary from 364 ± 8 Ma for the host gneiss to 350 ± 4 Ma for kyanite eclogite. The combined U-Pb and REE data interpreted in conjunction with observed CL domains and inclusion suites suggest that (1) Caledonian metamorphic zircon formed by both new zircon growth and recrystallization, (2) UHP metamorphism occurred near the end of the Caledonian collision, and (3) the 30–50

*Corresponding author e-mail: wmcclell@uidaho.edu.

McClelland, W.C., Power, S.E., Gilotti, J.A., Mazdab, F.K., and Wopenka, B., 2006, U-Pb SHRIMP geochronology and trace-element geochemistry of coesite-bearing zircons, North-East Greenland Caledonides, *in* Hacker, B.R., McClelland, W.C., and Liou, J.G., eds., Ultrahigh-pressure metamorphism: Deep continental subduction: Geological Society of America Special Paper 403, p. 23–43, doi: 10.1130/2006.2403(02).

m.y. span of ages records long residence times at eclogite-facies conditions for the UHP rocks of North-East Greenland. This spread in observed ages is interpreted to be characteristic of metamorphic rocks that have experienced relatively long (longer than 10 m.y.) residence times at UHP conditions.

Keywords: ultrahigh-pressure, coesite, U-Pb SHRIMP, Caledonides, Greenland.

INTRODUCTION

Subduction of continental material to depths of 100–120 km within collisional orogenic belts is widely accepted, based on the preservation of coesite and microdiamonds as inclusions in eclogite-facies minerals (Chopin, 2003, and references therein). Most ultrahigh-pressure (UHP) terranes lie in the footwall or subducted slab of the orogen (Michard et al., 1995; Hacker et al., 2000; Avigad et al., 2003). This geometry permits models based on buoyancy principles, in which dense mantle or oceanic material drags attached continental material to anomalous depths during subduction. Upon break off of the entire slab or delamination of the crust from the lithospheric mantle, the more buoyant continental material can be exhumed to normal crustal levels (Chemenda et al., 1996; Burov et al., 2001; Doin and Henry, 2001; Gerya et al., 2002; Roselle and Engi, 2002). In contrast, UHP metamorphic terranes in the overriding plate of collisional orogens, such as the Greenland Caledonides, carry significant implications for geodynamic models of collisional orogens and require alternatives to the popular continental subduction model (e.g., Ryan, 2001). The age of metamorphism is one of the most important parameters in defining models for formation and exhumation of UHP terranes in these different settings. Comparison of the ages of UHP metamorphism in the Western Gneiss Region of the Scandinavian Caledonides at 410–400 Ma (Carswell et al., 2003; Root et al., 2004) with the Greenland Caledonides at ca. 360 Ma (Gilotti et al., 2004) clearly suggests that the timing and duration of UHP metamorphism varies in different settings within an orogen.

The North-East Greenland eclogite province (Gilotti, 1993) contains widespread evidence for high-pressure metamorphism at 410–390 Ma (Brueckner et al., 1998; Elvevold and Gilotti, 2000). Evidence for UHP metamorphism in the North-East Greenland eclogite province was recognized by the presence of polycrystalline quartz pseudomorphs after coesite preserved in garnet and omphacite (Gilotti and Ravna, 2002). This paper documents the presence of coesite as inclusions in zircon from the same eclogites and host gneisses. The age of UHP metamorphism was reported as 360 ± 5 Ma, ~40 m.y. younger than high-pressure metamorphism observed elsewhere in the North-East Greenland eclogite province (Gilotti et al., 2004). This paper provides additional definitive evidence for the timing of UHP metamorphism in North-East Greenland.

Recent studies have demonstrated the importance of conducting in situ U-Pb analyses in conjunction with cathodoluminescence (CL) imaging and analysis of inclusion suites to link age information with UHP metamorphism (e.g., Hermann et al., 2001; Katayama et al., 2001; Liu et al., 2002, 2005; Kaneko et al., 2003; Yang et al., 2003). Three analytical techniques were employed to link zircon ages with UHP metamorphic conditions in this study: (1) Coesite was identified in zircons with laser Raman spectroscopy; (2) U-Pb ages were established by ion microprobe for domains defined by variation in CL intensities; and (3) rare earth element (REE) geochemistry of the CL-defined domains was obtained in an effort to tie the age determinations to UHP metamorphism by using flat heavy (H) REE patterns and the lack of a negative Eu anomaly in metamorphic zircon as a proxy for zircon growth at eclogite-facies conditions (Rubatto and Hermann, 2003).

GEOLOGICAL SETTING

The North-East Greenland eclogite province is preserved as the structurally highest sheet in a west-directed thrust belt developed along the Laurentian margin during the Caledonian collision with Baltica (Fig. 1; Higgins and Leslie, 2000; Higgins et al., 2004). The province is part of the Laurentian continental basement and is largely composed of quartzofeldspathic gneisses derived from 2.0 to 1.8 Ga deformed, calc-alkaline batholiths and crosscutting 1.74 Ga granitoids (Kalsbeek et al., 1993; Hull et al., 1994; Kalsbeek, 1995). Mafic rocks form meter- to kilometer-scale lenses and layers within the quartzofeldspathic gneisses, and many of them preserve a high-pressure mineralogy. Common lithologies include: eclogite sensu stricto, garnet clinopyroxenite, garnet websterite, websterite, and coronitic metagabbro (Gilotti, 1993, 1994; Gilotti and Elvevold, 1998; Lang and Gilotti, 2001). Protoliths of the eclogite-facies rocks were pre-Caledonian mafic dikes, mafic to ultramafic intrusions, and mafic xenoliths in the Paleoproterozoic calc-alkaline batholiths (Gilotti, 1993, 1994; Brueckner et al., 1998).

Two strike-slip shear zones divide the North-East Greenland eclogite province into western, central, and eastern blocks (Fig. 1). The vast majority of the high-pressure rocks in the eclogite province record medium-temperature (600–750 °C), high-pressure (1.5–2.3 GPa) metamorphic conditions (Brueckner et al., 1998; Elvevold and Gilotti, 2000) typical of a continental eclogite terrane. Spatial variation in pressure and temperature across the North-East Greenland eclogite province has yet to be discerned, in part due to the paucity of assemblages that are amenable to robust thermobarometry. In contrast, the Western Gneiss Region of Norway, a similar terrane on the Baltica margin, shows a steady increase in temperature

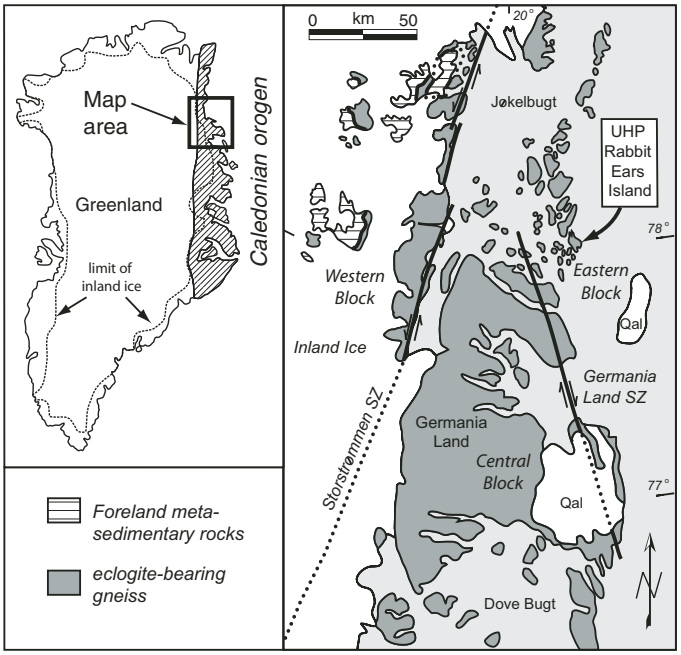

Figure 1. Simplified geologic map of the North-East Greenland eclogite province showing the ultrahigh-pressure (UHP) locality on an island in Jøkelbugt informally known as Rabbit Ears Island. SZ—subduction zone.

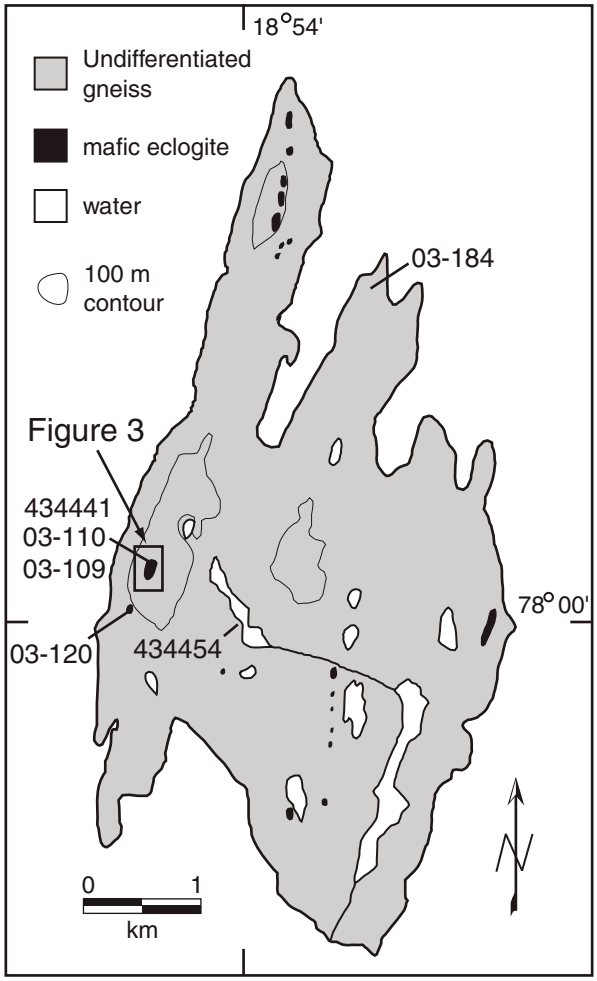

Figure 2. Geological map of Rabbit Ears Island showing location of samples mentioned in text.

toward the west (Griffin et al., 1985). The age of eclogite-facies metamorphism in the central and western blocks ranges from ca. 410–390 Ma (Gilotti et al., 2004).

Ultrahigh-pressure metamorphism is currently known from a small island in the eastern block, informally referred to as Rabbit Ears Island (Figs. 1 and 2; Gilotti and Ravna, 2002). Eclogite pods range from 1 to 50 m in width and 1 to >100 m in length, and are located in relatively narrow zones that can be traced for several kilometers along strike (Fig. 2). The eclogite-rich zones are parallel to the dominant NNW-striking gneissosity in the host rocks, and are interpreted as boudinaged, layered mafic intrusions. Many of the boudins have a blocky shape with pegmatites and leucogranites filling boudin necks and boudin-normal fractures (Fig. 3). The majority of the mafic boudins on Rabbit Ears Island consists of decimeter-scale, interlayered kyanite eclogite, bimineralic eclogite, and garnet-rich quartzite. The layering is interpreted to be a primary feature inherited from a layered mafic intrusive protolith. The eclogitic layers contain a foliation defined by kyanite, garnet, and omphacite that is parallel to that in the surrounding host gneisses; the layering and the foliation are isoclinally folded. The host rocks contain minor metapelite, but are mainly quartzofeldspathic orthogneisses that vary from mafic to more felsic compositions at the decimeter to 100 m scales. In contrast to the amphibole-bearing gneisses that dominate most other areas of the North-East Greenland eclogite province, abundant clinopyroxene is found in the host gneisses, indicating better preservation of the eclogite-facies history on Rabbit Ears Island.

Gilotti and Ravna (2002) identified microstructural and geothermobarometric features indicative of UHP metamorphism in the kyanite eclogites and their host gneisses. The microstructures include polycrystalline quartz inclusions with radial fractures in garnet, omphacite, and kyanite. Palisade quartz forms an outer rim around very finely recrystallized quartz in a number of inclusions, which is a diagnostic feature of pseudomorphs after coesite (Chopin and Sobolev, 1995; Hacker and Peacock, 1995). Polycrystalline quartz rods and single-quartz crystals with radial fractures are more abundant. Geothermobarometry on the garnet + omphacite + kyanite + quartz/coesite + phengite assemblage, using the Ravna and Terry (2004) calibration, returned temperatures in excess of 950 °C and pressures well into the coesite stability field (Gilotti and Ravna, 2002). The temperature may be overestimated and the pressure underestimated because of the difficulty in finding pristine phengite. The garnet-clinopyroxene equilibria line (calculated using Ravna, 2000) intersects the garnet + clinopyroxene

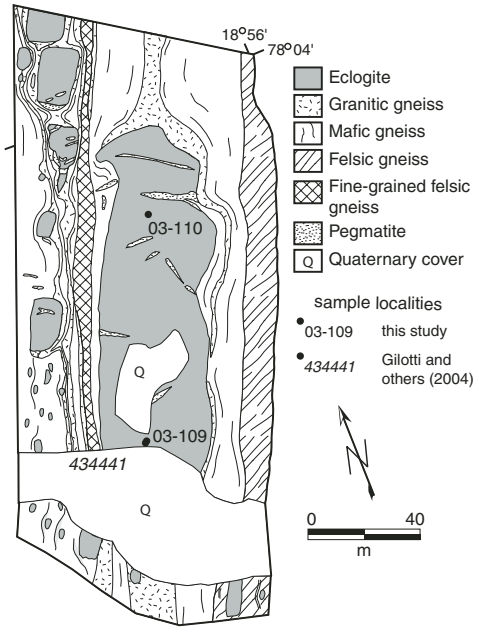

Figure 3. Detailed geological map of blocky, layered eclogite boudins surrounded by different gneissic lithologies, with two of the coesite-bearing kyanite eclogite sample locations shown. Pegmatites, emplaced during boudinage, cut the eclogite blocks at high angles, and granitic gneiss fills the boudin necks.

+ phengite equilibria at even higher temperatures, and is considered unreliable due to the assumption that all Fe is ferrous. Coesite, a major index mineral for UHP metamorphism, has now been identified in these rocks, leaving no doubt about their UHP provenance (see following).

Sample Description

Four samples from Rabbit Ears Island are now known to contain coesite. Three of the samples are from kyanite eclogite layers in mafic eclogite boudins, and the fourth sample is from the quartzofeldspathic host gneiss. The samples were collected during field work in 2003; their locations are shown on Figures 2 and 3. Minerals in thin section were identified using a petrographic microscope aided by energy dispersive analysis (EDS) on the JEOL 5600 scanning electron microscope (SEM) housed at Stanford University, Stanford, California.

Kyanite Eclogite

Samples 03-109 and 03-110 are from different kyanite eclogite layers within a 40 × 140 m blocky boudin (Fig. 3). Sample 03-109 is from the same exact location as 434441, the kyanite eclogite described by Gilotti and Ravna (2002) and dated by Gilotti et al. (2004; see their Figure 2f for a photomicrograph of the mineral assemblage). Kyanite eclogite sample 03-120 was collected from a similar banded eclogite boudin ~500 m south of 03-109. All three samples are medium grained, and contain the eclogite-facies assemblage garnet + omphacite + kyanite + quartz/coesite + phengite + rutile + zircon. The high-pressure assemblage is best preserved as inclusions in garnet and zircon. Polycrystalline and single-crystal quartz inclusions with radial fractures are abundant in garnet, but also occur in omphacite and kyanite. Millimeter-scale, elongate garnets lie parallel to the foliation defined by compositional layering and aligned omphacite, kyanite, and amphibole. Zircons occur enclosed in kyanite or along grain boundaries of other high-pressure phases (Fig. 4A). The samples have experienced variable amounts of retrogression, with 03-120 being the best preserved. Characteristic retrograde features include: diopside + plagioclase symplectites after omphacite; plagioclase ± amphibole halos around kyanite, garnet, and omphacite; biotite + plagioclase symplectites after phengite; and green amphibole directly replacing omphacite and as isolated poikioblastic crystals in the matrix.

Host Gneiss

The eclogite blocks are surrounded by interlayered mafic to felsic quartzofeldspathic gneisses (e.g., Fig. 3). Sample 03-184 was collected from quartzofeldspathic gneiss in an area that lacks boudinaged eclogite blocks (Fig. 2) but consists of decimeter-scale garnet-clinopyroxene–rich layers isoclinally folded with garnet-bearing felsic gneiss. The main high-pressure minerals—garnet + clinopyroxene + kyanite—are preserved throughout, but modal quartz + plagioclase vary considerably from layer to layer. The diopsidic clinopyroxene has a ragged, skeletal texture. Garnet and zircon preserve inclusions of the high-pressure mineral assemblage. As in the mafic rocks, zircon generally is enclosed in kyanite (Fig. 4C) but also occurs at grain boundaries of other high-pressure phases. Very fine-grained symplectites of amphibole + plagioclase surround kyanite and garnet; retrograde green amphibole is also abundant. Gilotti and Ravna (2002) calculated P = 2.5 GPa and T = 826 °C from kyanite + omphacite + quartz + phengite inclusions preserved in a single garnet from a sample collected at another host gneiss locality (434454; Fig. 2) that is much more strongly retrogressed than 03-184; they considered this to record a point on the retrograde path.

SAMPLE PREPARATION AND RAMAN SPECTROSCOPY

Analytical Methods

Zircons were separated from samples of kyanite eclogite, quartzofeldspathic orthogneiss, and one paragneiss by standard crushing and gravimetric techniques. The zircon separates were placed in alcohol and examined under a binocular microscope for handpicking of inclusion-bearing grains. The selected zircons from both the eclogites and the gneisses were clear, subspherical grains, ranging from 50 to 400 μm in diameter. Approximately 220 grains with 1–5 inclusions per grain from each of eight samples were mounted on double-sided adhesive tape on glass plates. All visible inclusions were analyzed by in situ laser Raman spectroscopy at the Department of Earth and

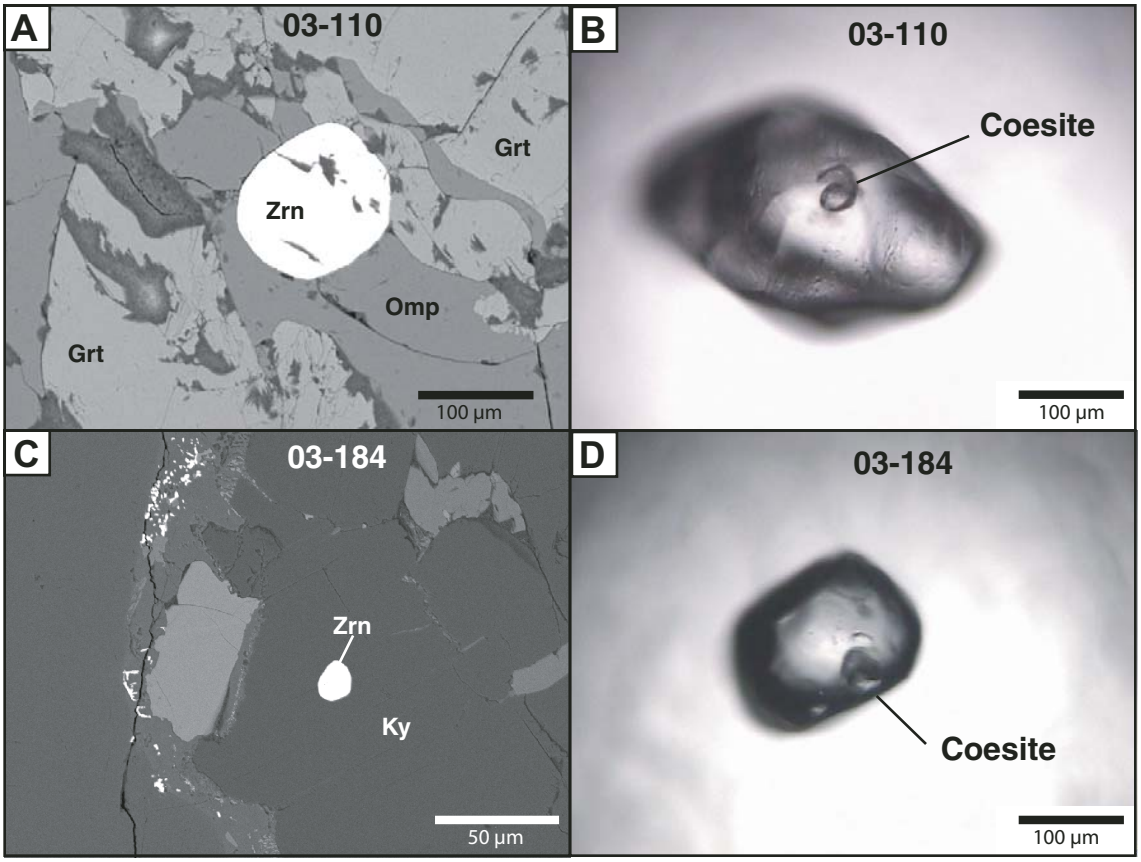

Figure 4. Backscattered-electron (A, C) and transmitted-light (B, D) images of zircon grains from eclogite and host gneiss. Eclogite sample 03-110: (A) Large, spherical zircon (Zrn) within garnet (Grt) and omphacite (Omp). (B) Subhedral, ovoid zircon with coesite inclusion (grain 56, Fig. 6). Host gneiss sample 03-184: (C) Small zircon in kyanite (Ky). (D) Spherical zircon with coesite inclusion (grain 48, Fig. 6). Coesite inclusions were identified via Raman microprobe analysis (see Fig. 5). Mineral abbreviations are after Kretz (1983).

Planetary Sciences, Washington University, St. Louis, Missouri. The instrument used was an integrated, fiber-optically coupled microscope-spectrometer-detector Raman microprobe system (see van Zuilen et al., 2005, for instrumental details). The 532 nm laser beam used to excite the Raman scattering was focused to ~1 µm, which allowed pinpoint analysis of individual phases within an inclusion.

Results

Zircons from all samples are morphologically ovoid to soccer-ball shaped, consistent with their origin in high-grade metamorphic rocks (Vavra et al., 1999; Schaltegger et al., 1999). Inclusion suites in over 1700 zircons were analyzed, and six coesite grains were identified in four different samples. Four coesite inclusions were found in zircon from the kyanite eclogites: one from 03-109, two from 03-110 (Fig. 4B), and one in 03-120. The coesites are round, 17–45 µm in diameter, and darker than the surrounding zircon matrix. We identified two coesite inclusions in the quartzofeldspathic host gneiss sample 03-184 (Fig. 4D). Zircons in the gneiss are on average larger than those found in the eclogites, and the coesite inclusions have diameters of 45 and 60 µm. After polishing, one coesite was seen in backscattered-electron (BSE) images to be a composite inclusion with the presence of omphacite confirmed by EDS.

Coesite can be unambiguously identified via Raman spectroscopy, because its Raman spectrum is distinctly different from any of the other SiO_2 polymorphs. Of specific relevance for the present study is that the Raman spectra of quartz and coesite are very different. Whereas the two most prominent peaks for quartz are at 464 and 204 Δcm^{-1}, the strongest peaks for coesite are at 524, 474, 428, 328, 270, and 207 Δcm^{-1}. The six coesite inclusions identified in the present study showed all the peaks for coesite and none of the quartz peaks (Fig. 5). Because the Raman scattering efficiency of zircon is much stronger compared to that of coesite, the peaks of the overlying zircon matrix are always detected (see Fig. 5), despite the fact that the method is close to confocal, and the laser beam is focused into the coesite inclusion below the sample surface. The strongest Raman peak for zircon is at 1005 Δcm^{-1} (not

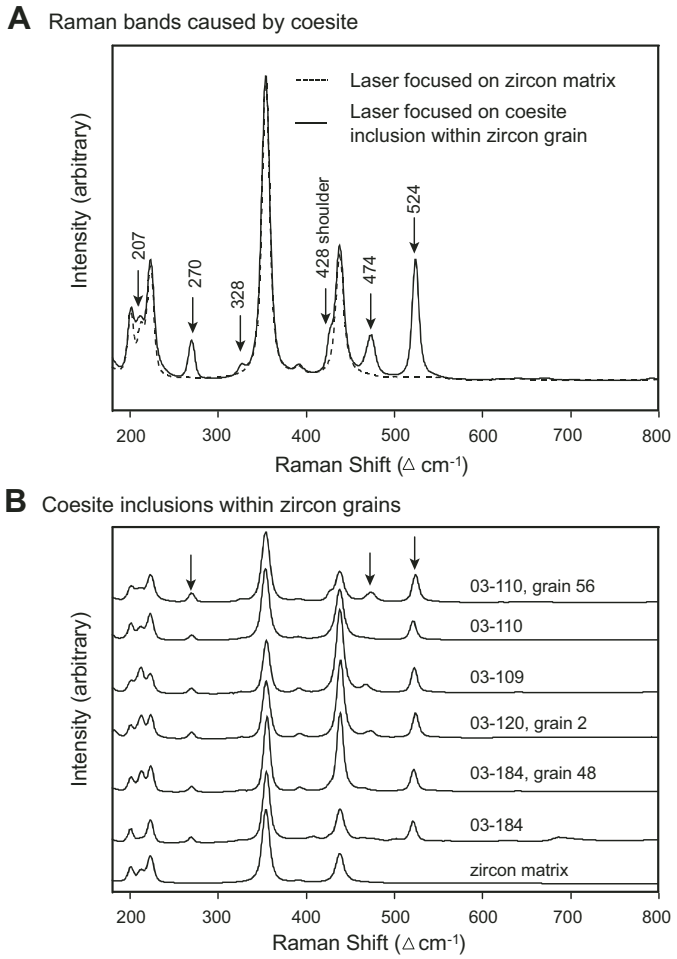

Figure 5. Raman spectra of coesite inclusions in zircon from eclogite and host gneiss from North-East Greenland. (A) Detailed spectrum generated with the laser focused on a coesite inclusion within zircon (solid line) compared to spectrum generated with laser focused on clean zircon matrix of grain from kyanite eclogite 03-110 shown in Figure 4B. The peaks caused by coesite are marked with arrows. (B) Spectra from six different coesite inclusions in zircon compared to the spectrum of the zircon host mineral. The most prominent peaks due to coesite are at 270, 474, and 524 Δcm^{-1} and are indicated with arrows. Grain numbers correspond to grains shown in Figure 6.

shown in Fig. 5), and characteristic weaker peaks occur at 438, 391, 354, 223, and 201 Δcm^{-1}. Figure 5B shows the spectra from six of the coesite grains found in the eclogites and gneiss, along with the spectrum for the zircon matrix. The Raman identification of the coesite inclusions within the isolated zircon grains of the North-East Greenland eclogite province region was straightforward for two reasons: (1) as mentioned already, none of the peaks for well-crystalline zircon overlap with the peaks for coesite, and (2) the zircons have low-U and low-Th concentrations, and thus their Raman spectra do not show any effects of metamictization. This means that the zircon peaks are very intense with narrow peak widths, which makes it easy to spectrally resolve them from the coesite peaks (see Fig. 5A).

U-Pb SHRIMP ANALYSIS

Analytical Methods

Zircons, including three of the coesite-bearing zircons, one each from samples 03-110, 03-120, and 03-184, were removed from glass slides used for Raman analysis, mounted in epoxy resin, and polished specifically to expose previously identified coesite inclusions and generally expose the interiors of all zircon grains. A coesite inclusion was successfully exposed in samples 03-110 and 03-184. CL images were collected for each sample using consistent settings to allow qualitative comparison between grains. Domains were defined within individual grains on the basis of variation in CL intensity. Although reasons for variation in luminescence in zircon are varied and poorly documented (see discussion in Nasdala et al., 2003), the CL domains generally coincide with variation in U concentration; low luminescent zones generally correspond with higher-U concentrations (e.g., Rubatto and Gebauer, 2000). Assuming that the CL domains may reflect different growth or recrystallization zones and therefore record age variations, the CL images were used to select spots for U-Pb analysis (Fig. 6). Zircons were analyzed for U-Pb isotopes on the SHRIMP-RG (sensitive high-resolution ion microprobe–reverse geometry) instrument at the U.S. Geological Survey–Stanford University Ion Probe Laboratory, Stanford, California. A 25–30-μm-diameter spot size was used for all analyses. The analytical routine followed Williams (1998), and data reduction utilized the SQUID program of Ludwig (2001a). The concentration of U was calibrated using zircon standard CZ3 (U = 550 ppm). Isotopic compositions were calibrated by replicate analyses of zircon standard R33 (419 Ma; Black et al., 2003). Zircons from the samples were analyzed during three sessions and from two different mounts. Calibration errors for $^{206}Pb/^{238}U$ ratios of R33 for the different analytical sessions were 0.81%, 0.39%, and 1.13% (2σ). The calculated external errors were incorporated when data from all sessions and mounts were compiled and compared. Most ages are younger than 1 Ga, so discussion and interpretation of analyses are based on $^{206}Pb/^{238}U$ ages calculated from ratios corrected for common Pb using the ^{207}Pb method. Ages older than 1 Ga are based on $^{207}Pb/^{206}Pb$ ages calculated from ratios corrected for common Pb using the measured ^{204}Pb. Common Pb compositions were estimated from Stacey and Kramers (1975).

Analyses were grouped according to domains determined by CL imaging, and ages were calculated as inverse-variance weighted mean $^{206}Pb/^{238}U$ ages with errors reported at the 95% confidence level. Age calculations and Tera-Wasserburg diagrams were generated with the Isoplot/Ex program of Ludwig (2001b). Analytical results are presented in Table 1 and plotted in Figures 7 and 8. The Caledonian $^{206}Pb/^{238}U$ ages calculated for each sample are plotted in order of decreasing age in Figure 8 to compare the age variation as a function of CL domain and the range of all analyses regardless of CL domain.

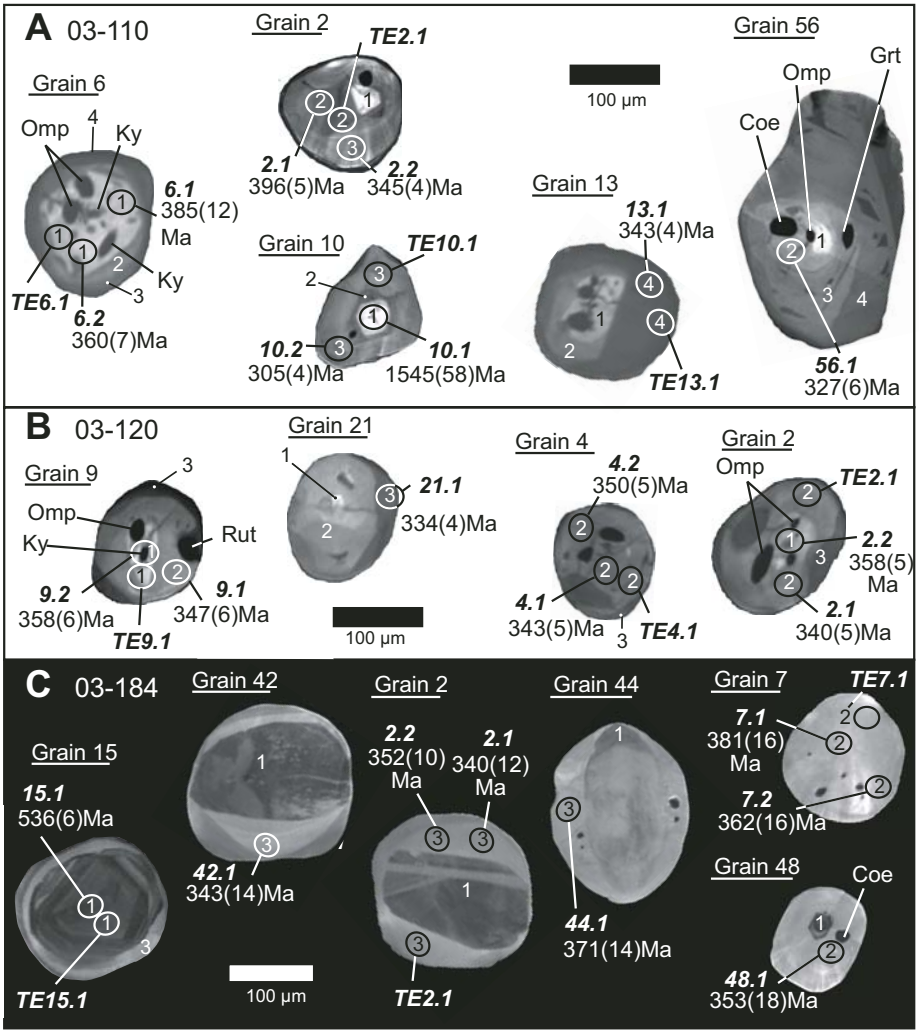

Figure 6. Representative cathodoluminescence (CL) images of subhedral to rounded zircon in dated coesite-bearing samples. Ellipses indicate sensitive high-resolution ion microprobe–reverse geometry (SHRIMP-RG) analysis spots labeled by grain number, spot number, and the corresponding U-Pb ages (±1σ Ma). Ellipses labeled TE indicate trace-element analysis spots. Numbers within the ellipses and on grains note assigned CL domain. Dark spots within the grains are generally inclusions. Where identified, inclusions are labeled with mineral abbreviations after Kretz (1983). (A) Zircons from kyanite eclogite 03-110 were divided into four CL domains. Coesite (Coe) occurs in domain 2 of grain 56. High-pressure/ultrahigh-pressure (HP/UHP) inclusions of kyanite (Ky), omphacite (Omp), and garnet (Grt) are also found in domains 1 and 2. (B) Zircons from kyanite eclogite 03-120 have three discernible CL domains. HP/UHP inclusions are abundant in domains 1 and 2. Coesite occurs in grain 2, but is not exposed at the polished surface. Rut—rutile. (C) Zircons from host gneiss 01-184 contain three CL domains. Grains 15, 42, 2, and 44 show a progression of recrystallization within and growth around older zircon. Grains 7 and 48, consisting almost entirely of low-U zircon, are assigned to domain 2. Grain 48 contains coesite.

Results

Zircons from UHP kyanite eclogite, sample 03-110, are subspherical, equant grains that exhibit four CL domains: (1) luminescent cores, (2) less luminescent cores and mantles, (3) less luminescent rims, and (4) low luminescent rims (e.g., grains 6 and 56; Fig. 6A). Not all domains are present in all grains (e.g., grains 2, 10, and 13; Fig. 6A) The CL domains generally correspond to variations in U concentration, although there is overlap. Domain 1 is characterized as low U (1–83 ppm), whereas both domains 2 and 3 have intermediate-U concentrations (10–243 ppm and 39–156 ppm, respectively). Domain 4 is high U (93–333 ppm) with respect to the other domains. Domain 1 contains inclusions of kyanite and omphacite and gives $^{206}Pb/^{238}U$ ages ranging from 328 to 1545 Ma. Th/U ratios range from 0.004 to 0.77, with the higher ratios associated with older ages. The three Proterozoic ages are interpreted to record the presence of igneous zircon from the mafic protolith, however, the inclusions of high-pressure eclogite-facies minerals point to new zircon growth in this domain during Caledonian metamorphism as well. Excluding the five oldest analyses and the youngest analysis, domain 1 gives a weighted mean

TABLE 1. U-Pb GEOCHRONOLOGIC DATA AND APPARENT AGES

Spot[a]		inclusions[a]	U (ppm)	Th (ppm)	Th/U	$^{206}Pb^{*b}$ (ppm)	$f^{206}Pb_c$ [b c]	$^{238}U/^{206}Pb$ [c]		$^{207}Pb/^{206}Pb$		$^{206}Pb/^{238}U$[d](Ma)		$^{207}Pb/^{206}Pb$[d] (Ma)	
Sample GL03-110 Kyanite eclogite															
Domain 1															
6.1	k,o		8	0.1	0.02	0.4	1.2	16.2549	(3)	0.05440	(15)	385	(12)		
6.2	k,o	TE	12	0.1	0.01	1.4	<0.01	17.4189	(2)	0.05358	(6)	360	(7)		
8.1			23	0.2	0.01	1.1	0.7	18.0141	(2)	0.05927	(6)	346	(7)		
10.1			28	20.8	0.77	6.7	1.8	3.6257	(4)	0.11137	(3)	1545	(58)	1777	(68)
12.1			24	0.1	0.004	1.2	0.5	17.3172	(2)	0.05768	(6)	360	(7)		
14.1		TE	28	0.6	0.02	1.4	0.7	16.8373	(2)	0.05970	(5)	369	(7)		
15.1		TE	81	46.0	0.59	10.7	4.2	6.4857	(2)	0.10382	(2)	888	(15)		
32.1		TE	35	0.7	0.02	4.6	0.3	15.1380	(2)	0.05711	(3)	411	(9)		
38.1			1	0.0	0.02	0.1	7.2	12.3794	(7)	0.11489	(17)	466	(34)		
41.1			55	1.9	0.36	2.6	0.5	18.4198	(2)	0.05746	(5)	339	(8)		
44.1			83	4.5	0.06	4.0	0.4	17.9496	(2)	0.05665	(3)	348	(7)		
46.1			41	0.9	0.02	2.1	<0.01	16.8986	(2)	0.05399	(5)	371	(9)		
49.1	o		37	0.4	0.01	3.2	0.1	9.9016	(4)	0.06116	(4)	620	(22)		
52.1			50	1.1	0.02	2.6	0.4	16.9024	(2)	0.05743	(4)	369	(8)		
53.1	k		81	3.9	0.05	3.7	0.9	18.9771	(2)	0.06019	(3)	328	(7)		
55.1			56	0.6	0.01	2.7	0.4	17.7373	(2)	0.05633	(4)	352	(8)		
Domain 2															
2.1		TE	127	0.4	0.003	6.9	<0.01	15.8447	(1)	0.05214	(3)	396	(5)		
3.1		TE	243	6.5	0.03	11.4	<0.01	18.2427	(1)	0.05330	(2)	344	(4)		
4.2		TE	35	0.1	0.004	4.0	0.5	17.6347	(1)	0.05741	(3)	354	(5)		
5.1			111	1.3	0.01	5.4	0.1	17.7011	(1)	0.05447	(3)	354	(5)		
5.2		TE	46	0.5	0.01	5.3	0.3	17.6140	(1)	0.05625	(3)	355	(5)		
9.1			235	13.0	0.06	11.5	<0.01	17.5660	(1)	0.05346	(2)	357	(5)		
9.2		TE	160	5.3	0.03	22.6	<0.01	14.2697	(2)	0.05334	(3)	438	(7)		
15.2			143	13.1	0.10	16.4	0.06	17.5035	(1)	0.05419	(2)	358	(4)		
16.1		TE	39	0.3	0.01	4.5	0.2	17.4394	(1)	0.05547	(3)	359	(5)		
20.1			27	0.3	0.01	2.9	0.5	18.5601	(2)	0.05727	(4)	337	(5)		
23.1			16	0.2	0.01	1.8	1.2	18.6515	(2)	0.06311	(5)	333	(6)		
27.1			19	0.2	0.01	2.2	0.2	17.3043	(2)	0.05571	(5)	361	(6)		
31.1			39	0.3	0.01	4.4	0.1	18.1876	(1)	0.05414	(3)	345	(5)		
33.1		TE	10	0.1	0.01	1.3	17.5	15.2433	(2)	0.19391	(6)	340	(10)		
35.1		TE	48	0.6	0.01	5.5	0.1	17.6307	(1)	0.05442	(3)	355	(5)		
36.1	o		101	1.7	0.02	4.3	<0.01	20.2729	(2)	0.05232	(3)	310	(6)		
40.1	k,r		87	1.1	0.01	3.8	0.05	19.6490	(2)	0.05316	(4)	320	(7)		
42.1			151	4.2	0.03	7.1	0.3	18.1292	(2)	0.05565	(3)	345	(7)		
43.1	o,g		116	1.7	0.02	5.6	<0.01	17.9717	(2)	0.05185	(3)	350	(7)		
47.1	o,g		115	0.9	0.01	5.5	0.4	18.0250	(2)	0.05696	(3)	347	(7)		
48.1			106	1.6	0.02	4.9	0.4	18.6003	(2)	0.05621	(3)	336	(7)		
50.1	o		142	1.9	0.01	6.8	<0.01	17.7810	(2)	0.05213	(3)	353	(7)		
51.1			93	1.5	0.02	4.6	0.1	17.4962	(2)	0.05439	(3)	358	(8)		
54.1	g,r		163	2.6	0.02	7. 5	<0.01	18.7929	(2)	0.05262	(3)	334	(7)		
56.1	c,o,g		162	2.4	0.02	7.3	0.4	19.1412	(2)	0.05633	(3)	327	(6)		
Domain 3															
1.1			73	0.4	0.016	3.5	0.3	18.1377	(1)	0.05536	(3)	345	(5)		
2.2			47	0.6	0.01	5.2	0.3	18.1151	(1)	0.05561	(3)	345	(5)		
7.1		TE	152	1.5	0.01	7.1	0.1	18.3497	(1)	0.05386	(2)	342	(4)		
10.2		TE	40	0.3	0.01	4.0	0.4	20.5736	(1)	0.05553	(3)	305	(4)		
17.1			44	0.6	0.01	4.7	0.5	18.5805	(1)	0.05744	(3)	336	(5)		
18.1			42	0.6	0.01	4.7	0.01	18.1148	(2)	0.05354	(4)	346	(6)		
19.1		TE	63	0.4	0.01	6.4	0.3	19.6381	(1)	0.05552	(3)	319	(4)		
22.1		TE	51	0.4	0.01	5.7	<0.01	18.2873	(1)	0.05278	(3)	343	(4)		
24.1			55	0.8	0.01	6.1	<0.01	18.2472	(1)	0.05169	(3)	345	(4)		
25.1			64	1.1	0.02	6.8	<0.01	18.9904	(1)	0.05248	(3)	331	(4)		
26.1			53	0.7	0.01	5.8	0.3	18.5007	(1)	0.05552	(3)	338	(4)		
28.1		TE	70	0.8	0.01	7.9	0.02	18.0255	(1)	0.05368	(2)	348	(4)		
29.1			156	7.8	0.05	17.1	<0.01	18.3346	(1)	0.05128	(2)	343	(4)		
30.1			119	5.5	0.05	13.3	0.3	18.0051	(1)	0.05572	(2)	347	(4)		
39.1	o		131	2.4	0.02	6.1	0.2	18.4613	(2)	0.05447	(3)	340	(7)		

(*continued*)

TABLE 1. U-Pb GEOCHRONOLOGIC DATA AND APPARENT AGES (*continued*)

Spot[a]	inclusions[a]	U (ppm)	Th (ppm)	Th/U	$^{206}Pb^{*b}$ (ppm)	$f^{206}Pb_c$ [b c]	$^{238}U/^{206}Pb$ [c]		$^{207}Pb/^{206}Pb$		$^{206}Pb/^{238}U$[d](Ma)		$^{207}Pb/^{206}Pb$[d] (Ma)	
Sample GL03-110 Kyanite eclogite (*continued*)														
Domain 4														
3.2		136	11.2	0.09	14.5	0.2	18.8303	(1)	0.05500	(2)	333	(4)		
4.1		280	17.6	0.07	13.5	0.3	17.8518	(1)	0.05602	(2)	350	(4)		
8.2		127	7.2	0.06	14.0	0.04	18.1764	(1)	0.05371	(2)	345	(4)		
11.1	TE	333	20.5	0.06	15.6	<0.01	18.3431	(1)	0.05206	(2)	343	(4)		
13.1	TE	292	14.3	0.05	13.7	0.2	18.2430	(1)	0.05491	(2)	343	(5)		
21.1		93	3.4	0.04	9.9	0.08	18.7613	(1)	0.05377	(2)	334	(4)		
34.1	TE	115	6.5	0.06	12.8	<0.01	17.9997	(1)	0.05304	(3)	349	(4)		
37.1		245	17.4	0.07	11.3	0.3	18.5986	(2)	0.05524	(2)	337	(6)		
45.1	o	276	79.9	0.30	11.9	<0.01	20.0455	(2)	0.05225	(2)	314	(6)		
Sample GL03-120 Kyanite eclogite														
Domain 1														
1.1	TE	3	0.2	0.06	0.17	1.98	17.2526	(4)	0.06956	(19)	356	(15)		
1.2		1	0.1	0.09	0.30	3.84	8.9651	(4)	0.09306	(10)	657	(27)		
2.2	c?	21	1.5	0.07	2.48	0.77	17.3577	(1)	0.05990	(4)	358	(5)		
3.2	k,o TE	11	0.5	0.05	1.61	4.60	14.0252	(2)	0.09256	(5)	424	(8)		
5.2		1	0.0	0.04	0.17	2.64	9.61130	(6)	0.08223	(14)	622	(36)		
6.2		8	0.3	0.03	0.86	0.81	18.0991	(2)	0.05988	(7)	344	(7)		
7.2	TE	9	0.1	0.01	1.08	0.45	16.7351	(3)	0.05772	(6)	372	(11)		
8.2		19	0.4	0.02	2.38	0.13	16.3188	(2)	0.05540	(5)	383	(6)		
9.2	k,o	18	0.9	0.05	2.30	9.16	15.9279	(2)	0.12754	(3)	358	(6)		
10.1	o	27	11.8	0.46	1.63	5.41	13.9766	(2)	0.09903	(4)	422	(10)		
12.1		24	0.6	0.03	1.15	1.59	17.9075	(2)	0.06615	(4)	345	(7)		
20.1	o	20	0.4	0.02	2.30	0.33	17.3365	(2)	0.05645	(4)	360	(6)		
Domain 2														
2.1	c? TE	42	0.5	0.01	1.94	0.33	18.4192	(2)	0.05591	(4)	340	(5)		
4.1	TE	61	0.9	0.02	2.87	0.19	18.2682	(1)	0.05484	(4)	343	(5)		
4.2	TE	29	1.0	0.03	3.29	0.46	17.8343	(1)	0.05724	(4)	350	(5)		
5.1		67	0.7	0.01	3.23	0.22	17.7068	(1)	0.05535	(3)	353	(5)		
6.1	TE	104	1.9	0.02	4.90	0.08	18.1742	(1)	0.05402	(3)	345	(5)		
8.1	TE	88	1.4	0.02	4.19	0.24	18.1015	(1)	0.05535	(3)	346	(5)		
9.1	r TE	35	0.2	0.01	1.64	<0.01	18.0992	(2)	0.05225	(5)	347	(6)		
10.2		56	3.6	0.07	5.41	0.89	20.9611	(2)	0.05947	(4)	298	(6)		
12.2		25	0.2	0.01	2.90	0.09	17.4055	(1)	0.05452	(8)	360	(5)		
14.1		96	2.4	0.03	4.49	0.31	18.3603	(1)	0.05580	(3)	341	(5)		
15.1	g	118	2.8	0.02	5.72	0.04	17.7597	(1)	0.05391	(3)	353	(5)		
16.1	o	76	1.7	0.02	3.66	0.61	17.8975	(1)	0.05838	(3)	348	(5)		
17.1		114	2.6	0.02	5.46	0.20	17.9681	(1)	0.05510	(3)	348	(5)		
18.1		7	0.3	0.04	0.84	7.77	16.1292	(2)	0.11633	(5)	358	(9)		
19.1	TE	24	1.0	0.04	2.79	0.23	17.4684	(1)	0.05562	(4)	358	(5)		
Domain 3														
3.1		170	12.3	0.08	8.10	0.04	17.9844	(1)	0.05381	(2)	349	(4)		
7.1		194	25.3	0.14	9.36	<0.01	17.7917	(1)	0.05243	(2)	353	(4)		
11.1		174	16.2	0.10	8.37	0.00	17.9124	(1)	0.05347	(2)	350	(4)		
13.1	TE	264	18.8	0.07	12.21	0.09	18.5511	(1)	0.05395	(2)	338	(4)		
13.2		111	7.9	0.07	12.24	0.37	18.2874	(1)	0.05633	(2)	342	(4)		
21.1		73	10.6	0.15	7.85	0.43	18.6957	(1)	0.05665	(3)	334	(4)		
Sample GL03-184 Quartzofeldpsathic orthogneiss														
Domain 1														
1.1	TE	324	92.8	0.30	16.1	0.5	17.3238	(1)	0.05758	(2)	360	(4)		
5.1	TE	202	64.5	0.33	28.0	4.0	6.1996	(1)	0.10319	(1)	928	(13)		
13.1	TE	233	60.9	0.27	13.1	1.7	15.2980	(1)	0.06868	(2)	401	(6)		
13.2		286	89.4	0.32	27.0	3.4	9.1126	(1)	0.08917	(2)	650	(10)		
14.1	TE	162	43.5	0.28	9.2	0.8	15.1282	(1)	0.06118	(5)	410	(5)		
14.2		200	52.4	0.27	13.8	2.0	12.4985	(2)	0.07328	(3)	487	(8)		
15.1	TE	159	21.2	0.14	12.2	2.4	11.2600	(1)	0.07787	(1)	536	(6)		
19.1		280	63.3	0.23	28.1	3.6	8.5442	(2)	0.09214	(1)	689	(14)		
47.1		244	71.2	0.30	53.0	3.0	3.9549	(2)	0.11506	(1)	1414	(25)	1888	(13)

(*continued*)

TABLE 1. U-Pb GEOCHRONOLOGIC DATA AND APPARENT AGES (*continued*)

Spot[a]	inclusions[a]	U (ppm)	Th (ppm)	Th/U	$^{206}Pb^{*b}$ (ppm)	$f^{206}Pb_c$ [b c]	$^{238}U/^{206}Pb$ [c]		$^{207}Pb/^{206}Pb$		$^{206}Pb/^{238}U$[d] (Ma)		$^{207}Pb/^{206}Pb$[d] (Ma)
Sample GL03-184 Quartzofeldpsathic orthogneiss (*continued*)													
Domain 2													
6.1	TE	124	46.2	0.39	6.2	0.4	17.0305	(2)	0.05751	(2)	366	(6)	
7.1	TE	3	0.04	0.01	0.2	1.4	16.2067	(4)	0.06551	(14)	381	(16)	
7.2		4	0.03	0.01	0.2	9.8	15.6155	(4)	0.13306	(10)	362	(16)	
12.2	o,g	3	0.25	0.08	0.2	3.5	17.2523	(5)	0.08173	(14)	351	(17)	
29.1	g	4	0.13	0.03	0.2	11.3	16.2505	(5)	0.14455	(11)	342	(19)	
35.1		10	0.41	0.04	0.5	0.3	16.4840	(4)	0.05649	(11)	379	(13)	
37.1		6	0.17	0.03	0.3	<0.01	16.4580	(4)	0.05130	(15)	382	(16)	
43.1	o	8	0.28	0.04	0.4	1.4	18.3248	(4)	0.06439	(11)	338	(14)	
48.1	c	4	0.07	0.02	0.2	1.4	17.5268	(5)	0.06456	(16)	353	(18)	
Domain 3													
1.2		13	1.5	0.11	0.6	0.8	19.1802	(3)	0.05945	(9)	325	(9)	
2.1	TE	8	0.12	0.02	0.4	2.9	17.9329	(4)	0.07625	(9)	340	(13)	
2.2		13	0.21	0.02	0.6	2.0	17.4480	(3)	0.06915	(8)	352	(10)	
3.1		11	0.14	0.01	0.6	2.1	16.9297	(2)	0.07069	(8)	362	(9)	
3.2	TE	4	0.05	0.01	0.2	0.9	15.4718	(4)	0.06194	(19)	400	(18)	
4.1	TE	5	0.04	0.01	0.2	1.5	16.9509	(4)	0.06607	(12)	364	(14)	
4.2		4	0.03	0.01	0.2	4.1	15.8982	(4)	0.08726	(13)	378	(17)	
6.2		55	10.1	0.19	2.7	<0.01	17.2571	(2)	0.05207	(4)	364	(7)	
8.1	k,o TE	12	0.81	0.07	0.6	<0.01	17.9200	(2)	0.04963	(8)	352	(8)	
8.2		16	2.2	0.14	0.8	2.3	17.8174	(3)	0.07194	(7)	344	(9)	
9.1	TE	6	0.02	0.00	0.3	1.9	18.1714	(3)	0.06851	(11)	339	(11)	
9.2		4	0.02	0.01	0.2	4.7	16.4092	(4)	0.09171	(11)	364	(16)	
10.1		8	0.12	0.01	0.4	<0.01	16.9760	(3)	0.05264	(10)	370	(10)	
10.2		6	0.06	0.01	0.3	3.2	16.4499	(4)	0.07946	(11)	369	(14)	
11.1		4	0.04	0.01	0.2	0.4	16.4500	(4)	0.05733	(15)	379	(14)	
11.2		3	0.02	0.01	0.2	3.7	16.0642	(5)	0.08410	(13)	375	(18)	
12.1	o,g TE	3	0.21	0.07	0.2	2.9	17.8303	(4)	0.07670	(15)	342	(15)	
16.1		23	0.30	0.01	1.2	0.7	16.6155	(2)	0.05966	(7)	374	(8)	
17.1		61	0.74	0.01	3.0	0.6	17.3918	(2)	0.05830	(4)	358	(7)	
18.1	TE	9	0.19	0.02	0.4	4.7	17.2758	(3)	0.09125	(8)	346	(11)	
20.1	g	3	0.13	0.05	0.1	6.4	16.1649	(5)	0.10516	(15)	363	(20)	
21.1		4	0.04	0.01	0.2	4.0	15.9107	(4)	0.08609	(12)	378	(17)	
22.1		7	0.23	0.03	0.4	2.3	15.7130	(3)	0.07256	(9)	389	(13)	
23.1	TE	13	0.68	0.06	0.6	0.6	18.3922	(3)	0.05804	(9)	339	(9)	
24.1		14	1.6	0.11	0.7	2.3	18.0829	(3)	0.07161	(8)	339	(10)	
25.1		14	0.23	0.02	0.7	0.5	16.9423	(3)	0.05766	(9)	368	(12)	
26.1		12	0.26	0.02	0.6	0.2	17.7569	(3)	0.05551	(11)	352	(12)	
27.1		73	33.4	0.47	5.9	3.1	10.5927	(2)	0.08422	(3)	564	(11)	
28.1		9	0.66	0.08	0.4	1.0	17.6688	(4)	0.06181	(10)	351	(13)	
30.1		8	0.35	0.05	0.4	1.1	16.0044	(4)	0.06345	(12)	386	(16)	
32.1		19	0.29	0.02	0.9	1.7	17.4747	(3)	0.06738	(8)	353	(11)	
33.1		67	3.9	0.06	3.2	0.4	17.6772	(2)	0.05662	(4)	353	(7)	
34.1	o	6	0.47	0.08	0.3	3.4	17.0636	(4)	0.08133	(10)	355	(15)	
36.1		6	0.62	0.10	0.3	1.1	15.9388	(4)	0.06301	(12)	388	(17)	
38.1		5	0.46	0.11	0.2	0.6	15.7824	(5)	0.05976	(14)	394	(19)	
39.1	g	2	0.15	0.07	0.2	5.6	12.1027	(6)	0.10208	(14)	484	(31)	
40.1		8	0.73	0.10	0.4	<0.01	17.4619	(4)	0.05054	(13)	360	(14)	
41.1		14	1.67	0.13	0.9	4.4	12.4698	(4)	0.09220	(6)	476	(18)	
42.1		7	0.32	0.05	0.3	0.7	18.1535	(4)	0.05930	(12)	343	(14)	
44.1		9	0.14	0.02	0.4	0.2	16.8239	(4)	0.05579	(12)	371	(14)	
45.1		17	2.1	0.13	0.8	0.0	17.8632	(3)	0.05352	(8)	351	(11)	
46.1		6	0.24	0.04	0.3	4.5	16.6088	(4)	0.09007	(11)	360	(16)	

Note: Zircon analyses were performed on the SHRIMP-RG ion microprobe at the USGS-Stanford Ion Probe Laboratory at Stanford University. Calibration concentrations and isotopic compositions were based on replicate analyses of CZ3 (550 ppm U), and R33 (419 Ma; Black and others, 2003). Analytical routine followed Williams (1998). Data reduction utilized Ludwig (2001a).

[a] See text for discussion of domains. Spots labeled as grain number-analysis number. Abbreviations: k = kyanite, o = omphacite; c = coesite; g = garnet; r = rutile; TE = trace element analysis in same domain; see Table 2. Coesite is queried for grain 2 of sample 03-120 because the inclusion is not exposed at the mount surface.

[b] Pb* denotes radiogenic Pb; Pb_c denotes common Pb; $f^{206}Pb_c = 100*(^{206}Pb_c/^{206}Pb_{total})$.

[c] Reported ratios are not corrected for common Pb. Errors are reported in parentheses as percent at the 1 σ level.

[d] $^{206}Pb/^{238}U$ ages calculated from ratios corrected for common Pb using ^{207}Pb. $^{207}Pb/^{206}Pb$ ages calculated from ratios corrected for common Pb using ^{204}Pb. Uncertainties in millions of years reported as 1σ.

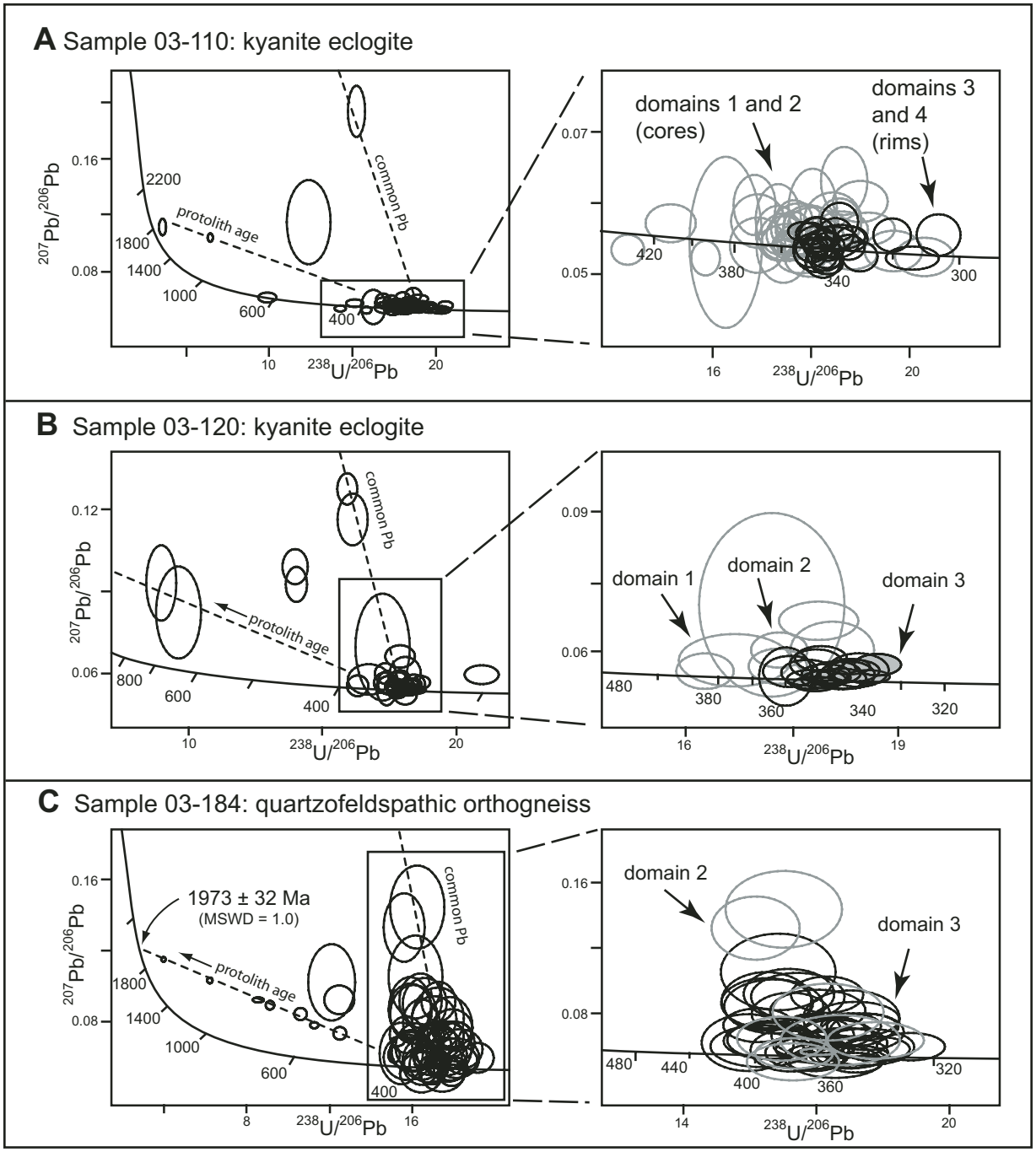

Figure 7. Tera-Wasserburg plots of sensitive high-resolution ion microprobe (SHRIMP) U-Pb data of zircon from kyanite eclogites (A) 03-110 and (B) 03-120, and (C) quartzofeldspathic host gneiss 03-184. Data are 1σ error ellipses uncorrected for common Pb. See text and Figure 8 for age interpretations. MSWD—mean square of weighted deviates.

$^{206}Pb/^{238}U$ age of 358 ± 9 Ma, with a mean square of weighted deviates (MSWD) of 2.7 (Fig. 8A). This age is within error of the 360 ± 5 Ma $^{206}Pb/^{238}U$ age reported from similarly low-U cores in zircon from a sample of kyanite eclogite, 434441, collected from the same pod at locality 03-109 (Fig. 3; Gilotti et al., 2004). Domain 2 contains inclusions of coesite, kyanite, omphacite, garnet, and rutile, has Th/U ratios of 0.003–0.10, and gives ages ranging from 310 to 438 Ma. The weighted mean $^{206}Pb/^{238}U$ age of domain 2 is 350 ± 4 Ma (MSWD = 2.5), after rejecting the two oldest and three youngest analyses on the basis of inheritance and Pb loss, respectively. Domains 3 and 4 distinguished in CL as having intermediate- and high-U con-

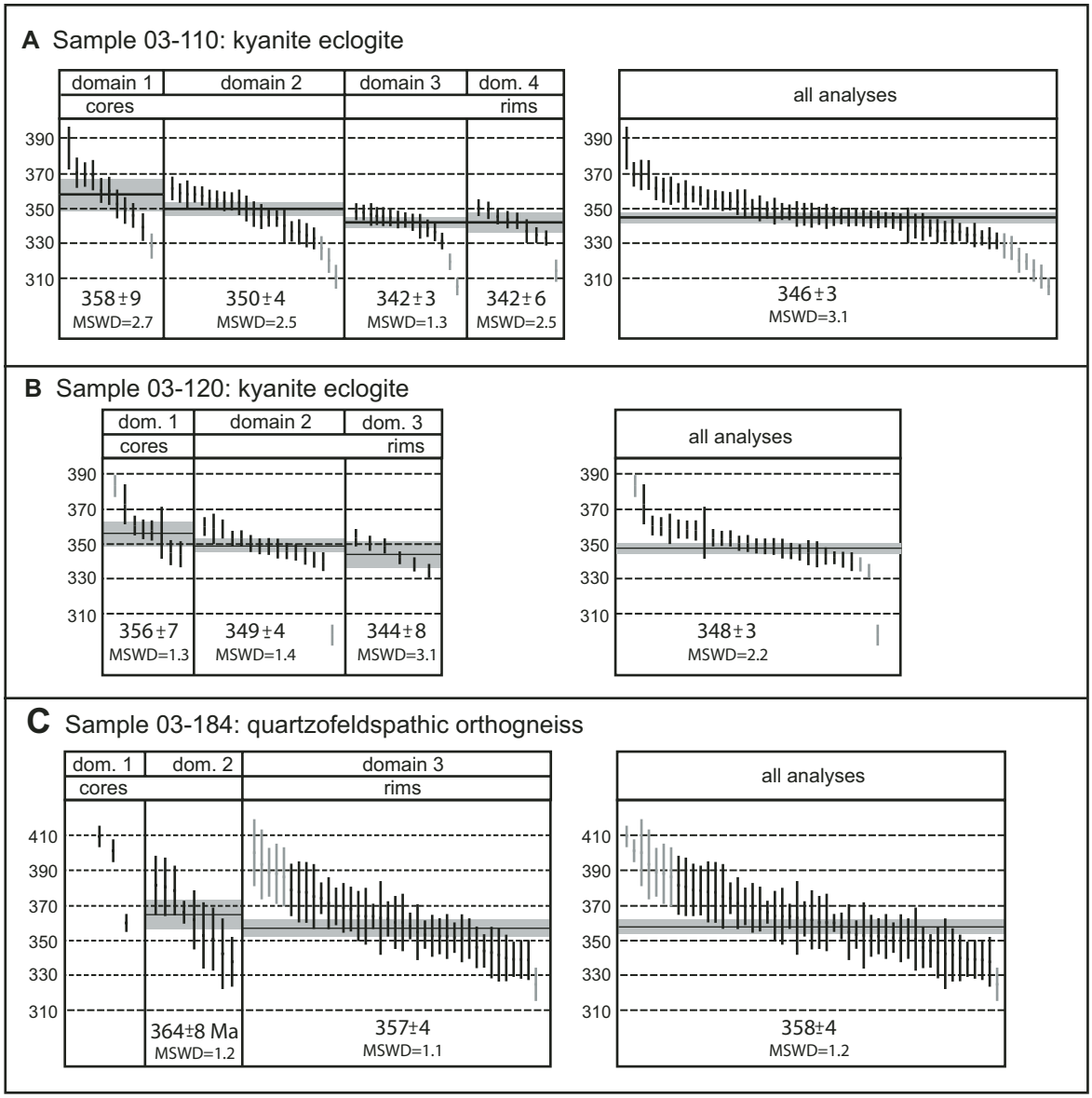

Figure 8. $^{206}Pb/^{238}U$ ages (in Ma) for kyanite eclogites (A) 03-110 and (B) 03-120, and (C) quartzofeldspathic host gneiss 03-184. Data are ^{207}Pb corrected, plotted with 1σ error bars, and sorted by age. Plots to the left show data separated according to cathodoluminescence (CL) domain and cite the weighted mean $^{206}Pb/^{238}U$ ages (95%confidence level), calculated with analyses shown in pale gray excluded. Plots on the right show the entire range of Caledonian ages within each sample. MSWD—mean square of weighted deviates.

centrations collectively give ages ranging from 305 to 350 Ma, with no significant difference in weighted mean age (342 ± 3 versus 342 ± 6 Ma; Fig. 8A) or Th/U ratio between the two domains. Assuming that the three youngest ages reflect Pb loss or younger rim growth during retrogression, the remaining 20 analyses from both domains 3 and 4 give a weighted mean $^{206}Pb/^{238}U$ age of 342 ± 3 Ma (MSWD = 1.6). Comparison of core domains 1 and 2 with rim domains 3 and 4 shows a systematic shift from older to younger ages (Figs. 7A and 8A). All analyses yield a weighted mean $^{206}Pb/^{238}U$ age of 346 ± 3 Ma (MSWD = 3.1).

Subspherical zircons separated from kyanite eclogite sample 03-120 are similar in character to those from 03-110, but have only three discernible CL domains (Fig. 6B). Domain 1 consists of low-U cores (1–27 ppm) that are not preserved in all grains (e.g., grain 4, Fig. 6B). The cores are mantled by zircon of intermediate-U concentration (7–118 ppm) assigned to domain 2. This domain is in turn overgrown by higher-U rims (73–264 ppm) of domain 3. The general core-to-rim increase in U concentration is matched by a general increase in Th concentration from 0.03 to 20 ppm, such that Th/U ratios of 0.005–0.46 are relatively constant throughout. Domain 1 contains kyanite and omphacite

inclusions, while the intermediate-U domain 2 encloses kyanite, omphacite, and garnet. The coesite inclusion in sample 03-120 (grain 2, Fig. 6B) was not exposed during polishing, so the coesite-bearing domain is not definitively known. Calculated $^{206}Pb/^{238}U$ ages from all domains range from 298 to 657 Ma (Figs. 7B and 8B). Excluding the five oldest core ages, which are interpreted to record mixing of protolith and metamorphic zircon signatures, domain 1 gives a weighted mean $^{206}Pb/^{238}U$ age of 356 ± 7 Ma (MSWD = 1.3). With the exclusion of the one anomalously young age, analyses from domain 2 provide a weighted mean age of 349 ± 4 Ma (MSWD = 1.4). The high-U rims of domain 3 yield a similar weighted mean age of 344 ± 8 Ma (MSWD = 3.1). Although there is a core-to-rim decrease in observed mean age, the significance cannot be assessed due to the overlapping errors for each domain (Fig. 8B). All analyses give a weighted mean $^{206}Pb/^{238}U$ age of 348 ± 3 Ma (MSWD = 2.2). The presence of similar inclusions in domains 1 and 2 indicates little change in metamorphic conditions during zircon growth or recrystallization, perhaps indicating that this sample remained at eclogite-facies conditions at least until 349 ± 4 Ma.

The quartzofeldspathic host gneiss sample, 03-184, yields subspherical grains with multiple CL domains (Fig. 6C), which are subdivided into high-U cores (domain 1; 159–324 ppm), low-U cores and mantles (domain 2; 3–124 ppm), and low-U rims (domain 3; 2–73 ppm). Some grains have oscillatory zoned higher-U domain 1 cores overgrown by distinct low-U rims of varying thickness, which are assigned to domain 3 (grain 15; Fig. 6C). Others show a gradation from well-defined cores, to cores with a network of lower-U veins and patchy, cloudy zones, which are attributed to recrystallization (grains 2, 42, and 44; Fig. 6C). Grains that appear as homogeneous lower-U grains are assigned to domain 2 (grains 7 and 48; Fig. 6C). The homogeneous low-U grains may represent either total recrystallization of igneous zircon, growth of metamorphic zircon, or both. Distinction between low-U grains of domain 2 and low-U rims of domain 3 becomes somewhat arbitrary as the rims thicken. The high-U cores have Th/U ratios of 0.14–0.33 characteristic of igneous zircon and $^{206}Pb/^{238}U$ ages ranging from 401 to 1414 Ma—excepting one younger age of 360 Ma (Figs. 7C and 8C). Regression of the six oldest data yields concordia intercept ages of 1973 ± 32 and 395 ± 19 Ma (MSWD = 1.0), respectively (Fig. 7C). The upper intercept age is interpreted as the emplacement age of the igneous protolith. Low-U grains assigned to domain 2 have Th/U ratios of 0.01–0.39, give $^{206}Pb/^{238}U$ ages ranging from 338 to 382 Ma and a weighted mean age of 364 ± 8 Ma (MSWD = 1.2). Coesite, omphacite, and garnet inclusions are observed in domain 2. Distinct low-U zircon rims of domain 3 contain inclusions of kyanite, omphacite, and garnet. Forty-three analyses of the domain 3 rims yield Th/U ratios of 0.004–0.47 and $^{206}Pb/^{238}U$ ages of 325–400 Ma, plus three older ages between 476 and 564 Ma. Inferring that the eight oldest rim ages represent mixtures of protolith and Caledonian zircon and the youngest age reflects Pb loss, the remaining 33 analyses give a weighted mean $^{206}Pb/^{238}U$ age of 357 ± 4 Ma (MSWD = 1.1) (Fig. 8C). The combined weighted mean $^{206}Pb/^{238}U$ age calculated for domains 2 and 3 is 358 ± 4 Ma (MSWD = 1.2).

SHRIMP-RG TRACE-ELEMENT ANALYSIS

Analytical Methods

Trace-element analyses for P, Y, REEs, Hf, Th, and U in zircon were carried out with the SHRIMP-RG using similar primary current and spot size to that used for U-Pb age determinations. In addition, by closing the Yα and collector slits, mass resolution was increased from M/ΔM = 6500–9500 to resolve the REE element peaks from interfering oxides (e.g., $^{141}Pr^{16}O$ from ^{157}Gd, and all comparable pairs).

The elemental peaks for ^{30}Si, P, Y, ^{96}Zr, ^{139}La, ^{140}Ce, ^{146}Nd, ^{147}Sm, ^{153}Eu, ^{157}Gd, Th, and ^{238}U were measured; for Pr, ^{163}Dy, ^{166}Er, ^{172}Yb, ^{175}Lu, and ^{180}Hf, the larger oxide peaks were measured. For each element, the average raw count rate for three measurement cycles was normalized to the average Si count rate and corrected for natural isotopic abundance. Periodic measurements of standard zircon from the Mud Tank carbonatite, Australia (Hoskin and Ireland, 2000), were compared to general calibration curves derived from analyses of NIST 611 glass (Pearce et al., 1997) to derive specific calibration factors for each element and to eliminate any matrix effect differences between the glass and zircon standards. Chondrite-normalized REE plots presented in Figure 9 use the chrondrite REE abundances of Anders and Grevesse (1989) multiplied by a factor of 1.36 (Korotev, 1996).

Results

Trace-element data from the three samples (Table 2) were collected from the same CL domains used in collection and interpretation of the U-Pb data; i.e., spot analyses for trace elements were made adjacent to but within the same domains as spots used for U-Pb analysis, as noted in Table 1. Chondrite-normalized REE values are plotted by domain in Figure 9. The trace-element patterns and variations discussed in the following are consistent with, but expand upon, earlier results reported from laser ablation–inductively coupled plasma–mass spectrometry (LA-ICP-MS) analyses of zircon from a kyanite eclogite on Rabbit Ears Island (Gilotti et al., 2004). SHRIMP-RG was used for this study due to its ability to analyze a smaller volume of material, and thus allow for better spatial resolution among CL domains than LA-ICP-MS. In general, all the samples have trace-element abundances and patterns characteristic of eclogite-facies metamorphic zircon (Rubatto, 2002; Hoskin and Schaltegger, 2003).

Three analyses of the low-U domain 1 cores in sample 03-110 show slightly negative to no Eu anomaly (Eu/Eu* = 0.4–0.9) and HREE patterns with $Lu_{(N)}/Gd_{(N)}$, calculated with chondrite-normalized values, ranging from 24 to 43 and $Lu_{(N)}$ = 25–43 (Fig. 9A). Domain 2, with intermediate-U concentra-

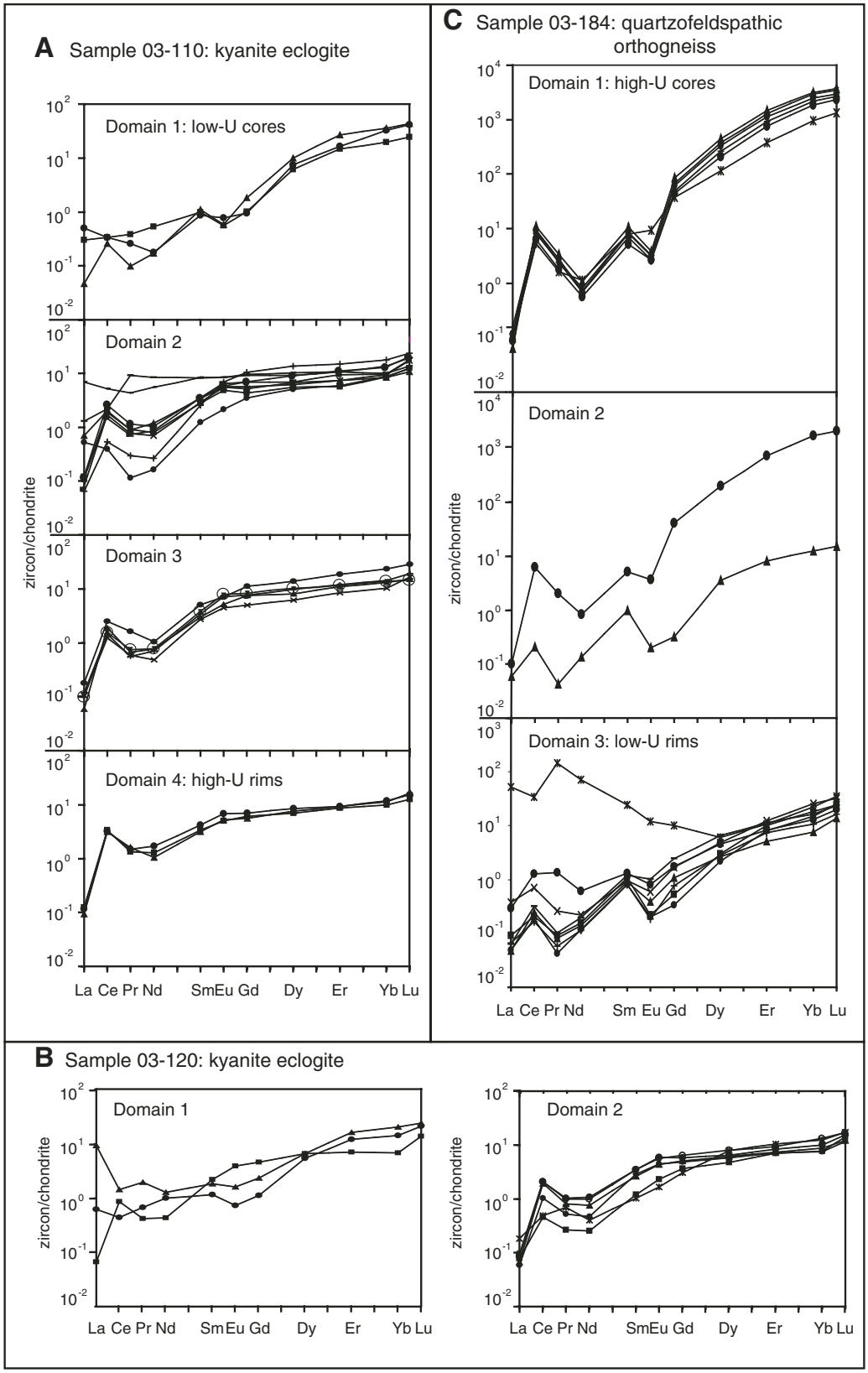

Figure 9. Chondrite-normalized rare earth element (REE) patterns for the different cathodoluminescence (CL) domains of zircons in the three U-Pb dated samples. Note the trend toward more consistent and flatter heavy (H) REE patterns toward the rims, as well as the absence of a Eu anomaly in the rims of the eclogites (03-110 and 03-120).

TABLE 2. ZIRCON TRACE ELEMENT DATA

Spot[a]	La	Ce	Nd	Sm	Eu	Pr	Gd	Dy	Er	Yb	Lu	Eu/Eu*	$Lu_{(N)}$[b]	$\frac{Lu_{(N)}}{Gd_{(N)}}$	P	Y	Hf	Th	U	U[c]
Sample GL03-110	Kyanite eclogite																			
Domain 1																				
6.1	0.10	0.28	0.33	0.20	0.04	0.05	0.27	2.00	3.20	4.32	0.81	0.6	25	24	32.5	12.3	19800	0.28	14	360
14.1	0.16	0.27	0.11	0.18	0.06	0.03	0.25	2.48	3.57	7.19	1.35	0.9	41	43	34.2	13.0	20500	0.55	9	28
32.1	0.01	0.21	0.11	0.22	0.04	0.01	0.48	3.28	5.80	7.85	1.42	0.4	43	24	19.2	19.7	15520	0.21	16	35
Domain 2																				
2.1	0.02	0.44	0.16	0.52	0.53	0.04	2.82	4.55	3.22	3.94	0.79	1.3	24	2	31.0	13.9	21100	0.18	100	127
3.1	0.04	2.16	0.64	0.69	0.44	0.14	1.83	2.95	2.33	2.80	0.64	1.2	19	3	26.6	10.0	19340	1.95	133	344
4.1	0.17	0.32	0.10	0.25	0.17	0.01	0.94	1.70	1.29	1.97	0.40	1.0	12	3	22.2	6.2	17400	0.09	40	35
5.1	0.04	1.55	0.49	0.57	0.37	0.11	1.16	1.85	1.23	1.92	0.41	1.4	13	3	24.4	6.2	20180	0.55	80	46
9.1	2.22	4.24	3.43	1.68	0.65	0.53	2.56	3.38	2.31	3.01	0.65	0.9	20	2	21.7	10.5	16650	7.72	287	160
15.1	0.04	1.40	0.44	0.58	0.42	0.09	1.41	2.27	1.59	2.11	0.58	1.4	18	3	26.6	7.4	20230	0.48	69	81
16.1	0.02	1.17	0.49	0.66	0.46	0.08	1.77	2.18	1.95	2.04	0.56	1.3	17	3	27.5	7.9	19750	0.32	64	39
33.1	0.42	1.82	5.22	1.67	0.65	1.13	2.45	3.04	2.31	2.21	0.46	1.0	14	2	22.1	9.6	18,570	0.25	53	10
35.1	0.23	1.65	0.73	0.69	0.43	0.11	1.53	2.06	1.59	1.88	0.36	1.3	11	2	25.4	7.3	19,210	0.67	84	48
Domain 3																				
7.1	0.05	1.99	0.62	0.99	0.53	0.19	2.93	4.47	3.99	5.13	0.93	0.9	28	3	26.8	17.2	16470	0.87	112	152
10.1	0.03	1.28	0.47	0.76	0.59	0.09	2.24	3.33	2.51	3.07	0.48	1.4	15	2	26.8	11.6	19450	0.42	80	40
19.1	0.03	0.97	0.28	0.53	0.33	0.07	1.31	2.00	1.80	2.23	0.54	1.2	16	3	24.5	7.5	18600	0.29	71	63
22.1	0.04	1.15	0.42	0.67	0.53	0.06	1.99	3.16	2.55	3.11	0.63	1.4	19	3	24.8	9.3	21540	0.63	116	51
28.1	0.02	1.50	0.45	0.58	0.38	0.08	1.98	2.61	2.34	2.86	0.49	1.1	15	2	27.6	9.2	18220	0.42	92	70
Domain 4																				
11.1	0.03	2.61	0.65	0.63	0.40	0.19	1.49	2.50	2.00	2.52	0.55	1.2	17	3	26.4	8.1	18340	5.66	178	333
13.1	0.04	2.66	1.04	0.84	0.52	0.18	1.89	2.79	2.01	2.65	0.51	1.2	15	2	26.7	9.2	19980	6.01	219	292
34.1	0.04	2.79	0.79	0.67	0.39	0.16	1.64	2.28	1.90	2.19	0.42	1.1	13	2	24.9	7.6	17440	7.31	179	115
Sample GL03-120	Kyanite eclogite																			
Domain 1																				
1.1	2.90	1.16	0.77	0.36	0.12	0.23	0.62	2.13	3.47	4.42	0.78	0.8	24	10	30.8	12.7	19660	0.30	5	3
3.1	0.20	0.35	0.60	0.23	0.05	0.08	0.30	1.77	2.55	3.08	0.69	0.6	21	19	24.5	9.0	19840	0.17	7	11
7.1	0.02	0.69	0.26	0.43	0.29	0.05	1.20	2.15	1.48	1.48	0.45	1.2	14	3	21.4	6.5	22110	0.28	32	9

(continued)

TABLE 2. ZIRCON TRACE ELEMENT DATA *(continued)*

Spot[a]	La	Ce	Nd	Sm	Eu	Pr	Gd	Dy	Er	Yb	Lu	Eu/Eu*	$Lu_{(N)}$[b]	$\frac{Lu_{(N)}}{Gd_{(N)}}$	P	Y	Hf	Th	U	U[c]
Sample GL03-120	Kyanite eclogite *(continued)*																			
Domain 2																				
2.1	0.02	0.84	0.29	0.58	0.34	0.06	1.31	1.91	1.54	1.66	0.39	1.2	12	2	20.6	6.0	22220	0.25	27	42
4.1	0.03	1.72	0.67	0.70	0.45	0.13	1.57	2.16	1.84	2.22	0.52	1.3	16	3	25.7	7.3	22450	0.55	52	61
6.1	0.02	1.61	0.47	0.53	0.34	0.10	1.35	2.03	1.60	1.95	0.40	1.2	12	2	21.8	6.8	20340	0.48	58	104
8.1	0.03	1.66	0.59	0.67	0.43	0.12	1.70	2.60	1.98	2.94	0.56	1.2	17	3	27.5	9.0	20400	0.61	63	88
9.1	0.02	0.38	0.16	0.24	0.18	0.03	0.99	1.59	1.52	1.73	0.47	1.1	14	4	24.0	6.9	21360	0.30	22	35
19.1	0.06	0.41	0.25	0.21	0.13	0.08	0.82	2.63	2.29	2.74	0.57	0.9	17	6	23.9	10.6	21350	0.3	6	24
Domain 3																				
13.1	0.05	2.68	0.96	0.73	0.40	0.17	1.56	1.98	1.81	1.89	0.37	1.1	11	2	19.6	7.9	12840	7.5	132	264
Sample GL03-184	Quartzofeldspathic orthogneiss																			
Domain 1																				
1.1	0.03	5.10	0.34	1.04	0.20	0.22	11.71	70	167	408	77	0.2	2320	53	256	597	13040	22	123	324
5.1	0.02	9.00	0.64	2.15	0.29	0.41	22.68	146	319	701	124	0.1	3750	44	282	841	20960	35	190	202
13.1	0.03	7.22	0.51	1.67	0.24	0.31	18.23	123	282	642	114	0.1	3460	51	267	754	20020	28	167	233
14.1	0.04	7.63	0.44	1.62	0.24	0.33	16.52	111	248	548	98	0.1	2980	48	231	669	20670	25	165	162
15.1	0.03	4.38	0.69	1.59	0.71	0.20	9.91	38	82	207	44	0.5	1330	36	101	231	12630	8.7	116	159
16.1	0.05	6.81	0.42	1.37	0.20	0.30	13.15	88	203	483	89	0.1	2680	54	188	545	20880	24	145	nd
Domain 2																				
6.1	0.03	4.93	0.51	0.99	0.27	0.24	10.61	63	150	359	67	0.3	2020	51	150	387	17140	15	76	55
7.1	0.02	0.17	0.08	0.20	0.02	0.01	0.08	1.15	1.73	2.72	0.49	0.4	15	47	28.0	7.0	23000	0.01	2	4
Domain 3																				
2.1	0.09	1.04	0.38	0.26	0.06	0.16	0.47	1.49	1.78	2.88	0.66	0.5	20	11	26.5	7.3	22900	0.11	6	8
3.1	0.02	0.20	0.09	0.18	0.03	0.01	0.29	0.88	1.11	1.67	0.46	0.4	14	13	19.3	4.2	23540	0.06	4	4
4.1	0.03	0.17	0.09	0.21	0.02	0.01	0.14	0.99	2.21	4.07	0.81	0.3	25	47	24.3	6.6	22680	0.03	3	4
8.1	16.80	28.11	44.54	4.90	0.90	17.40	2.67	2.02	2.34	5.01	1.15	0.8	35	3	28.7	7.5	24830	1.2	9	12
9.1	0.02	0.14	0.07	0.16	0.01	0.01	0.20	0.93	1.60	2.38	0.54	0.2	16	22	25.8	5.4	24080	0.04	3	4
12.1	0.02	0.15	0.07	0.16	0.02	0.01	0.09	0.72	1.74	3.35	0.83	0.4	25	75	26.6	5.2	25910	0.01	2	3
18.1	0.12	0.58	0.14	0.19	0.05	0.03	0.45	1.59	2.63	5.68	1.07	0.5	32	19	28.5	9.1	24460	0.36	5	9
23.1	0.02	0.26	0.12	0.24	0.08	0.01	0.65	2.16	2.44	3.66	0.79	0.6	24	10	27.1	8.7	28130	0.35	9	13

Note: All analyses were performed on the SHRIMP-RG ion microprobe at the USGS-Stanford Ion Probe Laboratory at Stanford University. All abundances expressed in ppm.
[a]Grain numbers and domains are the same as in Table 1.
[b]$Lu_{(N)}$ and $Gd_{(N)}$ values are chondrite-normalized.
[c]U concentration determined from domain by CZ3 during U/Pb analysis.

tions, is characterized by higher and more variable light (L) REE values, slightly positive to no Eu anomalies (Eu/Eu* = 0.9–1.4), generally positive Ce anomalies, and flat HREE patterns ($Lu_{(N)}/Gd_{(N)}$ = 2–4; $Lu_{(N)}$ = 11–24). Patterns observed for domains 3 and 4 are more systematic (Fig. 9A). The domains lack a negative Eu anomaly (Eu/Eu* = 0.9–1.4), have well-defined positive Ce anomalies, and flat HREE patterns ($Lu_{(N)}/Gd_{(N)}$ = 2–3; $Lu_{(N)}$ = 13–28). The variation observed in the REE patterns coincides reasonably well with the different CL domains.

Domain 1 zircon cores from kyanite eclogite 03-120 have characteristics similar to those observed in the previous sample: variable REE abundances, negative to no Eu anomaly (Eu/Eu* = 0.6–1.4), and flat HREE patterns ($Lu_{(N)}/Gd_{(N)}$ = 3–19; $Lu_{(N)}$ = 14–24). Patterns in domain 2 are more systematic, and are characterized by the absence of a Eu anomaly (Eu/Eu* = 0.9–1.3), positive Ce anomalies, and flat HREE patterns ($Lu_{(N)}/Gd_{(N)}$ = 2–6; $Lu_{(N)}$ = 11–17). No trace-element analyses were obtained from high-U rims of domain 3.

The REE signatures from zircons within the quartzofeldspathic gneiss are markedly different than those from the kyanite eclogites. The high-U cores of domain 1 have enriched HREE ($Lu_{(N)}/Gd_{(N)}$ = 36–54; $Lu_{(N)}$ = 1332–3751) and well-developed positive Ce anomalies and negative Eu anomalies (Eu/Eu* = 0.1–0.5). Domain 2 analyses are transitional between domains 1 and 3. Domain 3 has markedly depleted HREE ($Lu_{(N)}/Gd_{(N)}$ = 3–75; $Lu_{(N)}$ = 14–35) and smaller positive Ce anomalies and negative Eu anomalies (Eu/Eu* = 0.2–0.8). Domain 1 patterns are attributed to an igneous protolith signature, whereas domains 2 and 3 record growth and recrystallization during metamorphism.

DISCUSSION

The results of both the U-Pb and trace-element analyses on coesite-bearing zircon suites examined in this study generally vary as a function of CL domains, which in turn reflect a general variation in U concentration. In addition to establishing the timing of UHP metamorphism in North-East Greenland, interpretation of the results addresses several issues concerning the significance of U-Pb ages obtained for UHP rocks in other settings. These include: (1) to what extent do the metamorphic zircons represent recrystallization of existing zircons versus new zircon growth by precipitation, and (2) does the considerable spread in U-Pb ages observed from some UHP metamorphic zircons represent analytical scatter or geologically meaningful variation in age?

Recrystallization versus New Growth

Metamorphic zircon forms either by growth of new zircon or recrystallization of pre-existing zircon (Hoskin and Schaltegger, 2003, and references therein). In this study, growth of zircon as new grains and rims on xenocrystic cores is clearly established from inclusions of coesite, as well as kyanite, garnet, and omphacite, within the grains. New zircon must trap coesite during UHP metamorphism, because the coesite-to-quartz transition is thought to be extremely rapid. Experimental and theoretical considerations (Mosenfelder and Bohlen, 1997; Perrillat et al., 2003) predict that 100-μm-sized coesite crystals will transform to quartz in less than 1 m.y. at temperatures below 400 °C. Lenze et al. (2005) considered the transformation to be quasi-instantaneous on geologic time scales, based on experiments where coesite reverts to quartz within hours after rapid decompression from 3 GPa to 2.7 GPa at 800 °C. Once grown, zircon protects coesite inclusions from fluid infiltration that would have led to its transformation during high-temperature decompression (Mosenfelder et al., 2005). Complications may arise when quartz inclusions within igneous zircon are present (e.g., Gebauer et al., 1997), but in all cases, the timing of UHP metamorphism will be same or younger than the age of zircon that encloses the coesite. For the North-East Greenland samples, we unequivocally equate the presence of coesite inclusions with zircon growth at UHP conditions. New zircon formed through precipitation from anatectic melts, metamorphic fluids, or through subsolidus net-transfer reactions is not expected to contain inherited components. Therefore, the age of coesite-bearing zircon is interpreted to record the timing of zircon growth at UHP conditions.

Recrystallization of protolith zircon is signified by the retention of older isotopic or trace-element signatures (e.g., Rubatto, 2002; Puga et al., 2005). All of the samples in this study contain zircon grains with remnants of xenocrystic cores that record a Paleoproterozoic protolith age (Fig. 7). Inherited cores are best preserved in the host gneiss 03-184. CL textures, U-Pb ages, and REE analyses clearly record variable recrystallization of pre-existing zircon with new rim overgrowths (Fig. 6C). The core-to-rim variation in REE patterns in the host gneiss sample exemplifies the depletion of HREE, slightly negative to absent Eu anomaly, and persistent positive Ce anomaly that is characteristic of zircon recrystallized at subsolidus, high-grade metamorphic conditions (Hoskin and Black, 2000; Rubatto, 2002). In addition to the older ages obtained from the core region, five low-U rim analyses give older U-Pb ages (older than 390 Ma) and are interpreted to reflect an inheritance signature due to incomplete recrystallization. Similarly, a small number of low-U domain 1 cores in the kyanite eclogite samples yield older U-Pb ages thought to be a memory effect. Zircon suites from all three of the samples are interpreted to record both processes: recrystallization and new growth.

Spread in U-Pb Ages

The U-Pb ages vary smoothly from 370 to 330 Ma for kyanite eclogite and 390–330 Ma for the host gneiss (Fig. 8). The observed variation may be explained by analytical scatter, combined effects of inheritance and Pb loss, or a true variation in age. The 40–60 m.y. range in ages is not attributed to analytical

scatter, since the variation is similar in all samples, regardless of U concentration. There is a distinct break at the upper end of the range to older ages that clearly represent inheritance signatures. Similarly, younger ages that clearly reflect Pb loss or new growth during amphibolite-facies retrograde metamorphism are recognized as outliers in all of the samples (Fig. 8). For the remaining analyses, the mean ages of the various domains do decrease from core to rim as expected, although the domain ages generally overlap within analytical uncertainty. The REE patterns and inclusion suites indicate that the domains are unique as well. Data from kyanite eclogite sample 03-110 indicate that the low-U domain 1 cores record recrystallization and zircon growth during prograde eclogite-facies metamorphism at ca. 360 Ma. The disappearance of the slightly negative Eu anomaly between domains 1 and 2 may reflect complete removal of plagioclase during eclogitization. The appearance of coesite in the domain 2 zircon that mantles the low-U cores (Fig. 6A) establishes that the UHP metamorphism was ongoing at 350 ± 4 Ma. Subsequent rim growth occurred at 342 ± 4 Ma, perhaps in part during amphibolite-facies retrograde metamorphism. This progression of ages combined with the REE data is interpreted to record a true variation in zircon growth and recrystallization at eclogite-facies conditions at least to 350 Ma. The coesite-bearing domain from the host gneiss gives an older age of 364 ± 8 Ma. The difference in ages over relatively short distances as a function of lithology suggests that the timing of zircon recrystallization and growth varied according to fluid availability and zircon-forming net-transfer reactions. Assuming the range in ages is geologically meaningful, UHP metamorphism in North-East Greenland was ongoing by 370 Ma and continued through 350 Ma.

Geochronologic Implications

The inclusion suites in conjunction with the U-Pb and REE data indicate that the CL domains observed in the UHP zircons resulted from both new growth and recrystallization. Recrystallized zircon can give a mixed protolith plus metamorphic U-Pb signature, but this is much less likely for newly grown domains that contain eclogite-facies inclusions. Using this study as an example, this distinction generally cannot be made on the basis of U concentration or Th/U ratio. Nevertheless, ion microprobe techniques provide the spatial resolution to isolate domains of new growth from xenocrystic cores, as well as to recognize zones that record memory effects of the protolith due to incomplete recrystallization. The observed range in U-Pb ages in the Greenland eclogite-facies zircons is interpreted to reflect long-lived zircon crystallization and growth. The weighted mean of the entire range in this case masks the geological significance of the age spread.

The general differences between secondary ion mass spectrometry (SIMS) and isotope-dilution thermal-ionization mass spectrometry (ID-TIMS) analytical techniques are well documented and generally accepted (e.g., Davis et al., 2003; Parrish and Noble, 2003). In essence, there is a tradeoff between spatial resolution and precision. ID-TIMS analyses can establish a high-precision mean age for the timing of zircon recrystallization and growth, but it is difficult to avoid or isolate inheritance signatures that result from dissolution of xenocrystic material or partially recrystallized domains. SIMS analyses can spatially isolate different domains but have difficulty in establishing high-precision ages necessary to resolve slight variations in age. As an example, Root et al. (2004) argued that the observed 40 m.y. spread in SHRIMP ages on zircon from the Western Gneiss Region in Norway reflects inheritance. The inferred age for UHP metamorphism of 405–400 Ma is based on interpretation of slightly discordant chemical abrasion ID-TIMS data (see Mattinson, 2005, for analytical method). As illustrated by this study, the age variability defined by SHRIMP analyses may in fact record continuous zircon growth and recrystallization over a long time span. In this case, the ID-TIMS data would record the mean age of the zircon, with the slight discordance reflecting the memory effects of incompletely recrystallized protolith zircon.

Tectonic Implications

The long residence time at eclogite-facies conditions proposed for UHP rocks in the Greenland Caledonides differs substantially from the rapid subduction (Kaneko et al., 2003) and exhumation demonstrated for other UHP terranes (e.g., Hacker et al., 2003; Rubatto and Hermann, 2001; Lapen et al., 2003). The fast rates fit models incorporating return-flow concepts in a subduction channel to explain rapid exhumation (e.g., Chemenda et al., 1996). The long residence time at eclogite-facies conditions in the North-East Greenland eclogite province suggests that UHP terranes in the overriding plates of collisional orogens may be formed and exhumed by different mechanisms than those in the downgoing plate. Gilotti et al. (2004) showed that the North-East Greenland eclogite province experienced high-pressure metamorphism at ca. 410–390 Ma, but only the oldest ages observed in the host gneiss zircons in this study are consistent with this age. In this study, it was not possible to distinguish between recrystallized zones with slight retention of older components and new growth as early as 400 Ma in the UHP zircons. This may, however, be the case for the host gneiss sample (Fig. 8). If the 385–410 Ma ages that were rejected in calculation of the weighted mean ages in fact do not contain inheritance, the age range over which the UHP terrane experienced eclogite-facies conditions would be extended to ca. 400–350 Ma. Nevertheless, our interpretation of the combined U-Pb, REE, and inclusion suite data is that the UHP rocks in the North-East Greenland eclogite province stayed at eclogite-facies high-pressure to UHP conditions for 10–20 m.y.

CONCLUSIONS

The combined results of the SHRIMP U-Pb and REE analyses, and inclusion suite analysis on kyanite eclogite and host gneiss samples suggest that UHP metamorphic zircon

forms due to both recrystallization of protolith zircons and new growth. Although a few older ages represent incomplete resetting during recrystallization, the span of 370–350 Ma ages from kyanite eclogite is inferred to record continuous growth and thus residence time at eclogite-facies to UHP conditions. The older age span observed for the host gneiss indicates that new zircon growth initiated at least 10 m.y. earlier in the host gneisses than in kyanite eclogites. Variations in ages observed in UHP terranes may, therefore, reflect differences in bulk composition rather than differences in timing of metamorphism. The long residence times indicated for the North-East Greenland eclogites are interpreted to be indicative of UHP metamorphism within the overriding plate of a collisional orogen.

ACKNOWLEDGMENTS

National Science Foundation grants to Gilotti (EAR-0208236) and McClelland (EAR-0208158) supported the field work and analytical work, respectively. We are grateful to the Danish Polar Center for coordinating the logistics for the field work, and to the staff at the Danmarkshavn weather station for their generous help and hospitality. We thank Ben Hallett for his help with the detailed mapping and sampling. Helpful reviews were provided by Brad Hacker, Andrew Kylander-Clark, Chris Mattinson, and Dave Root.

REFERENCES CITED

Anders, E., and Grevesse, N., 1989, Abundances of the elements: Meteoritic and solar: Geochimica et Cosmochimica Acta, v. 53, p. 197–214, doi: 10.1016/0016-7037(89)90286-X.

Avigad, D., Chopin, C., and Le Bayon, R., 2003, Thrusting and extension in the southern Dora-Maira ultra-high-pressure massif (Western Alps): View from below the coesite-bearing unit: The Journal of Geology, v. 111, p. 57–70, doi: 10.1086/344664.

Black, L.P., Kamo, S.L., Williams, I.S., Mundil, R., Davis, D.W., Korsch, R.J., and Foudoulis, C., 2003, The application of SHRIMP to Phanerozoic geochronology; a critical appraisal of four zircon standards: Chemical Geology, v. 200, p. 171–188, doi: 10.1016/S0009-2541(03)00166-9.

Brueckner, H.K., Gilotti, J.A., and Nutman, A., 1998, Caledonian eclogite facies metamorphism of Early Proterozoic protoliths from the North-East Greenland eclogite province: Contributions to Mineralogy and Petrology, v. 130, p. 103–120, doi: 10.1007/s004100050353.

Burov, E., Jolivet, L., Le Pourhiet, L., and Poliakov, A., 2001, A thermomechanical model of exhumation of high pressure (HP) and ultra-high pressure (UHP) metamorphic rocks in Alpine-type collision belts: Tectonophysics, v. 342, p. 113–136, doi: 10.1016/S0040-1951(01)00158-5.

Carswell, D.A., Brueckner, H.K., Cuthbert, S.J., Mehta, K., and O'Brien, P.J., 2003, The timing of stabilisation and the exhumation rate for ultra-high pressure rocks in the Western Gneiss Region of Norway: Journal of Metamorphic Geology, v. 21, p. 601–612, doi: 10.1046/j.1525-1314.2003.00467.x.

Chemenda, A.I., Mattauer, M., and Bokun, A.N., 1996, Continental subduction and a mechanism for exhumation of high pressure metamorphic rocks: New modeling, field data from Oman: Earth and Planetary Science Letters, v. 143, p. 173–182, doi: 10.1016/0012-821X(96)00123-9.

Chopin, C., 2003, Ultrahigh-pressure metamorphism: Tracing continental crust into the mantle: Earth and Planetary Sciences Letters, v. 212, p. 1–14, doi: 10.1016/S0012-821X(03)00261-9.

Chopin, C., and Sobolev, N.V., 1995, Principal mineralogic indicators of UHP in crustal rocks, *in* Coleman, R.G., and Wang, X., eds., Ultrahigh-pressure metamorphism: Cambridge, Cambridge University Press, p. 96–131.

Davis, D.W., Williams, I.S., and Krogh, T.E., 2003, Historical development of zircon geochronology, *in* Hanchar, J.M., and Hoskin, P.W.O., eds., Zircon: Reviews in Mineralogy and Geochemistry, v. 53, p. 145–181.

Doin, M.P., and Henry, P., 2001, Subduction initiation and continental crust recycling: The roles of rheology and eclogitization: Tectonophysics, v. 342, p. 163–191, doi: 10.1016/S0040-1951(01)00161-5.

Elvevold, S., and Gilotti, J.A., 2000, Pressure-temperature evolution of retrogressed kyanite eclogites, Weinschenk Island, North-East Greenland Caledonides: Lithos, v. 53, p. 127–147, doi: 10.1016/S0024-4937(00)00014-1.

Gebauer, D., Schertl, H.-P., Brix, M., and Schreyer, W., 1997, 35 Ma old ultrahigh-pressure metamorphism and evidence for very rapid exhumation in the Dora Maira Massif, Western Alps: Lithos, v. 41, p. 5–24.

Gerya, T.V., Stöckhert, B., and Perchuk, A.L., 2002, Exhumation of high-pressure metamorphic rocks in a subduction channel: A numerical simulation: Tectonics, v. 21, p. 6-1–6-19, doi: 10.1029/2002TC001406.

Gilotti, J.A., 1993, Discovery of a medium-temperature eclogite province in the Caledonides of North-East Greenland: Geology, v. 21, p. 523–526, doi: 10.1130/0091-7613(1993)021<0523:DOAMTE>2.3.CO;2.

Gilotti, J.A., 1994, Eclogites and related high-pressure rocks from North-East Greenland: Grønlands Geologiske Undersøgelse Rapport, v. 162, p. 77–90.

Gilotti, J.A., and Elvevold, S., 1998, Partial eclogitization of the Ambolten gabbro-norite North-East Greenland Caledonides: Schweizerische Mineralogische und Petrographische Mitteilungen, v. 78, p. 273–292.

Gilotti, J.A., and Ravna, E.J.K., 2002, First evidence for ultrahigh-pressure metamorphism in the North-East Greenland Caledonides: Geology, v. 30, p. 551–554.

Gilotti, J.A., Nutman, A.P., and Brueckner, H.K., 2004, Devonian to Carboniferous collision in the Greenland Caledonides: U-Pb zircon and Sm-Nd ages of high-pressure and ultrahigh-pressure metamorphism: Contributions to Mineralogy and Petrology, v. 148, p. 216–235, doi: 10.1007/s00410-004-0600-4.

Griffin, W.L., Austrheim, H., Brastad, K., Bryhni, I., Krill, A.G., Krogh, E.J., Mørk, M.-B.E., Qvale, H., and Tørudbakken, B., 1985, High-pressure metamorphism in the Scandinavian Caledonides, *in* Gee, D.G., and Sturt, B.A., eds., The Caledonide orogen—Scandinavia and related areas: Chichester, John Wiley, p. 783–801.

Hacker, B.R., and Peacock, S.M., 1995, Creation, preservation, and exhumation of UHPM rocks, *in* Coleman, R.G., and Wang, X., eds., Ultrahigh-pressure metamorphism: Cambridge, Cambridge University Press, p. 159–181.

Hacker, B.R., Ratschbacher, L., Webb, L., McWilliams, M., Calvert, A., Dong, S., Wenk, H.-R., and Chateigner, D., 2000, Exhumation of ultrahigh-pressure continental crust in east central China: Late Triassic–Early Jurassic tectonic unroofing: Journal of Geophysical Research, v. 105, p. 13,339–13,364.

Hacker, B.R., Andersen, T.B., Root, D.B., Mehl, L., Mattinson, J.M., and Wooden, J.L., 2003, Exhumation of high-pressure rocks beneath the Solund Basin, Western Gneiss Region of Norway: Journal of Metamorphic Geology, v. 21, p. 613–629, doi: 10.1046/j.1525-1314.2003.00468.x.

Hermann, J., Rubatto, D., Korsakov, A., and Shatsky, V.S., 2001, Multiple zircon growth during fast exhumation of diamondiferous, deeply subducted continental crust (Kokchetav Massif, Kazakhstan): Contributions to Mineralogy and Petrology, v. 141, p. 66–82.

Higgins, A.K., and Leslie, A.G., 2000, Restoring thrusting in the East Greenland Caledonides: Geology, v. 28, p. 1019–1022, doi: 10.1130/0091-7613(2000)028<1019:RTITEG>2.3.CO;2.

Higgins, A.K., Henriksen, N.H., Jepsen, H.F., Kalsbeek, F., Thrane, K., Elvevold, S., Escher, J.C., Frederiksen, K.S., Gilotti, J.A., Jones, K., Leslie, A.G., Smith, M.P., Kinny, P.D., and Watt, G.R., 2004, The foreland-propagating architecture of the East Greenland Caledonides

72°–75°N: Journal of the Geological Society of London, v. 161, p. 1009–1026.

Hoskin, P.W.O., and Black, L.P., 2000, Metamorphic zircon formation by solid-state recrystallization of protolith igneous zircon: Journal of Metamorphic Geology, v. 18, p. 423–439, doi: 10.1046/j.1525-1314.2000.00266.x.

Hoskin, P.W.O., and Ireland, T.R., 2000, Rare earth element chemistry of zircon and its use as a provenance indicator: Geology, v. 28, p. 627–630, doi: 10.1130/0091-7613(2000)028<0627:REECOZ>2.3.CO;2.

Hoskin, P.W.O., and Schaltegger, U., 2003, The composition of zircon and igneous and metamorphic petrogenesis, *in* Hanchar, J.M., and Hoskin, P.W.O., eds., Zircon: Reviews in Mineralogy and Geochemistry, v. 53, p. 29–62.

Hull, J.M., Friderichsen, J.D., Gilotti, J.A., Henriksen, N., Higgins, A.K., and Kalsbeek, F., 1994, Gneiss complex of the Skærfjorden region, North-East Greenland: Grønlands Geologiske Undersøgelse Rapport, v. 162, p. 35–51.

Kalsbeek, F., 1995, Geochemistry, tectonic setting, and poly-orogenic history of Paleoproterozoic basement rocks from the Caledonian fold belt of North-East Greenland: Precambrian Research, v. 72, p. 301–315, doi: 10.1016/0301-9268(94)00097-B.

Kalsbeek, F., Nutman, A.P., and Taylor, P.N., 1993, Palaeoproterozoic basement province in the Caledonian fold belt of North-East Greenland: Precambrian Research, v. 63, p. 163–178, doi: 10.1016/0301-9268(93)90010-Y.

Kaneko, Y., Katayama, I., Yamamoto, H., Misawa, K., Ishikawa, M., Rehman, H.U., Kausar, A.B., and Shiraishi, K., 2003, Timing of Himalayan ultrahigh-pressure metamorphism: Sinking rate and subduction angle of the Indian continental crust beneath Asia: Journal of Metamorphic Geology, v. 21, p. 589–599.

Katayama, I., Maruyama, S., Parkinson, C.D., Terada, K., and Sano, Y., 2001, Ion microprobe U-Pb zircon geochronology of peak and retrograde stages of ultrahigh-pressure metamorphic rocks from the Kokchetav Massif, northern Kazakhstan: Earth and Planetary Science Letters, v. 188, p. 185–198, doi: 10.1016/S0012-821X(01)00319-3.

Korotev, R.L., 1996, A self-consistent compilation of elemental concentration data for 93 geochemical reference samples: Geostandards Newsletter, v. 20, p. 217–245.

Kretz, R., 1983, Symbols for rock-forming minerals: The American Mineralogist, v. 68, p. 277–279.

Lang, H.M., and Gilotti, J.A., 2001, Plagioclase replacement textures in partially eclogitised gabbros from the Sanddal mafic-ultramafic complex, Greenland Caledonides: Journal of Metamorphic Geology, v. 19, p. 497–515, doi: 10.1046/j.0263-4929.2001.00325.x.

Lapen, T.J., Johnson, C.M., Baumgartner, L.P., Mahlen, N.J., Beard, B.L., and Amato, J.M., 2003, Burial rates during prograde metamorphism of an ultra-high-pressure terrane: An example from Lago di Cignana, western Alps, Italy: Earth and Planetary Science Letters, v. 215, p. 57–72, doi: 10.1016/S0012-821X(03)00455-2.

Lenze, A., Stöckhert, B., and Wirth, R., 2005, Grain scale deformation in ultrahigh-pressure metamorphism—An indicator of rapid phase transformation: Earth and Planetary Science Letters, v. 229, p. 217–230, doi: 10.1016/j.epsl.2004.10.012.

Liu, F., Xu, Z., Liou, J.G., Katayama, I., Masago, H., Maruyama, S., and Yang, J., 2002, Ultra-high pressure mineral inclusions in zircons from gneissic core samples of the Chinese Continental Scientific Drilling Site in eastern China: European Journal of Mineralogy, v. 71, p. 180–188.

Liu, F., Liou, J.G., and Xu, Z., 2005, U-Pb SHRIMP ages recorded in the coesite-bearing zircon domains of paragneisses in the southwestern Sulu terrane, eastern China: New interpretation: The American Mineralogist, v. 90, p. 790–800, doi: 10.2138/am.2005.1677.

Ludwig, K.R., 2001a, Squid version 1.02: A user's manual: Berkeley Geochronology Center Special Publication, v. 2, p. 1–22.

Ludwig, K.R., 2001b, Isoplot/EX version 2.49: A geochronological toolkit for Microsoft Excel: Berkeley Geochronology Center Special Publication, no. 1a, p. 1–55.

Mattinson, J.M., 2005, Zircon U-Pb chemical abrasion (CA-TIMS) method: Combined annealing and multi-step partial dissolution analysis for improved precision and accuracy of zircon ages: Chemical Geology, v. 220, p. 47–66, doi: 10.1016/j.chemgeo.2005.03.011.

Michard, A., Henry, C., and Chopin, C., 1995, Structures in UHPM rocks: A case study from the Alps, *in* Coleman, R.G., and Wang, X., eds., Ultrahigh-pressure metamorphism: Cambridge, Cambridge University Press, p. 132–158.

Mosenfelder, J.L., and Bohlen, S.R., 1997, Kinetics of the coesite to quartz transformation: Earth and Planetary Science Letters, v. 153, p. 133–147, doi: 10.1016/S0012-821X(97)00159-3.

Mosenfelder, J.L., Schertl, H.P., Smyth, J.R., and Liou, J.G., 2005, Factors in the preservation of coesite: The importance of fluid infiltration: The American Mineralogist, v. 90, p. 779–789, doi: 10.2138/am.2005.1687.

Nasdala, L., Zhang, M., Kempe, U., Panczer, G., Gaft, M., Andrut, M., and Plötze, M., 2003, Spectroscopic methods applied to zircon, *in* Hanchar, J.M., and Hoskin, P.W.O., eds., Zircon: Reviews in Mineralogy and Geochemistry, v. 53, p. 427–467.

Parrish, R.R., and Noble, S.R., 2003, Zircon U-Th-Pb geochronology by isotope dilution–thermal ionization mass spectrometry (ID-TIMS), *in* Hanchar, J.M., and Hoskin, P.W.O., eds., Zircon: Reviews in Mineralogy and Geochemistry, v. 53, p. 183–213.

Pearce, N.J.G., Perkins, W.T., Westgate, J.A., Gorton, M.P., Jackson, S.E., Neal, C.R., and Cheney, S.P., 1997, New data for National Institute of Standards and Technology 610 and 612 glass reference materials: Geostandards Newsletter, v. 21, p. 115–144.

Perrillat, J.P., Daniel, I., Lardeaux, J.M., and Cardon, H., 2003, Kinetics of the coesite-quartz transition: Application to the exhumation of ultrahigh-pressure rocks: Journal of Petrology, v. 44, p. 773–788, doi: 10.1093/petrology/44.4.773.

Puga, E., Fanning, C.M., Nieto, J.M., and Dıaz de Federico, A., 2005, Recrystallization textures in zircon generated by ocean-floor and eclogite-facies metamorphism: A cathodoluminescence and U-Pb SHRIMP study, with constraints from REE elements: Canadian Mineralogist, v. 43, p. 183–202.

Ravna, E.J.K., 2000, The garnet-clinopyroxene Fe^{2+}-Mg geothermometer: An updated calibration: Journal of Metamorphic Geology, v. 18, p. 211–219, doi: 10.1046/j.1525-1314.2000.00247.x.

Ravna, E.J.K., and Terry, M.P., 2004, Geothermobarometry of UHP and HP eclogites and schists—An evaluation of equilibria among garnet-clinopyroxene-kyanite-phengite-coesite/quartz: Journal of Metamorphic Geology, v. 22, p. 579–592, doi: 10.1111/j.1525-1314.2004.00534.x.

Root, D.B., Hacker, B.R., Mattinson, J.M., and Wooden, J.L., 2004, Zircon geochronology and ca. 400 Ma exhumation of Norwegian ultrahigh-pressure rocks: An ion microprobe and chemical abrasion study: Earth and Planetary Science Letters, v. 228, p. 325–341, doi: 10.1016/j.epsl.2004.10.019.

Roselle, G.T., and Engi, M., 2002, Ultrahigh pressure (UHP) terrains: Lessons from thermal modeling: American Journal of Science, v. 302, p. 410–441.

Rubatto, D., 2002, Zircon trace element geochemistry: Partitioning with garnet and the link between U-Pb ages and metamorphism: Chemical Geology, v. 184, p. 123–138, doi: 10.1016/S0009-2541(01)00355-2.

Rubatto, D., and Gebauer, D., 2000, Use of cathodoluminescence for U-Pb zircons dating by ion microprobe: Some examples from the Western Alps, *in* Pagel, M., Barbin, V., Blanc, P., and Ohnenstetter, D., eds., Cathodoluminescence in geosciences: Berlin, Springer, p. 373–400.

Rubatto, D., and Hermann, J., 2001, Exhumation as fast as subduction?: Geology, v. 29, p. 3–6, doi: 10.1130/0091-7613(2001)029<0003:EAFAS>2.0.CO;2.

Rubatto, D., and Hermann, J., 2003, Zircon formation during fluid circulation in eclogites (Monviso, Western Alps): Implications for Zr and Hf budget in subduction zones: Geochimica et Cosmochimica Acta, v. 67, p. 2173–2187, doi: 10.1016/S0016-7037(02)01321-2.

Ryan, P.D., 2001, The role of deep basement during continent-continent collision: A review, *in* Miller, J.A., Holdsworth, R.E., Buick, I.S., and Hand, M., eds., Continental reactivation and reworking: Geological Society of London Special Publication 184, p. 39–55.

Schaltegger, U., Fanning, C.M., Günther, D., Maurin, J.C., Schulmann, K., and Gebauer, D., 1999, Growth, annealing and recrystallization of zircon and preservation of monazite in high-grade metamorphism: Conventional and in-situ U-Pb isotope, cathodoluminescence and microchemical evidence: Contributions to Mineralogy and Petrology, v. 134, p. 186–201, doi: 10.1007/s004100050478.

Stacey, J.S., and Kramers, J.D., 1975, Approximation of terrestrial lead isotope evolution by a two-stage model: Earth and Planetary Science Letters, v. 26, p. 207–221, doi: 10.1016/0012-821X(75)90088-6.

van Zuilen, M.A., Mathew, K., Wopenka, B., Lepland, A., Marti, K., and Arrhenius, G., 2005, Nitrogen and argon isotopic signatures in graphite from the 3.8-Ga-old Isua Supracrustal Belt: Southern West Greenland: Geochimica et Cosmochimica Acta, v. 69, p. 1241–1252, doi: 10.1016/j.gca.2004.08.033.

Vavra, G., Schmid, R., and Gebauer, D., 1999, Internal morphology, habit and U-Th-Pb microanalysis of amphibolite-to-granulite facies zircons: Geochronology of the Ivrea Zone (Southern Alps): Contributions to Mineralogy and Petrology, v. 134, p. 380–404, doi: 10.1007/s004100050492.

Williams, I.S., 1998, U-Pb by ion microprobe, *in* McKibben, M.A., Shanks, W.C., and Ridley, W.I., eds., Applications of microanalytical techniques to understanding mineralizing processes: Society of Economic Geologists Reviews Economic Geology, v. 7, p. 1–35.

Yang, J.S., Wooden, J.L., Wu, C.L., Liu, F.L., Xu, Z.Q., Shi, R.D., Katayama, I., Liou, J.G., and Maruyama, S., 2003, SHRIMP U-Pb dating of coesite-bearing zircon from the ultrahigh-pressure metamorphic rocks, Sulu terrane, east China: Journal of Metamorphic Geology, v. 21, p. 551–560, doi: 10.1046/j.1525-1314.2003.00463.x.

Manuscript Accepted by the Society 21 September 2005

Printed in the USA

Geological Society of America Special Papers

U-Pb SHRIMP geochronology and trace-element geochemistry of coesite-bearing zircons, North-East Greenland Caledonides

William C. McClelland, Siobhán E. Power, Jane A. Gilotti, et al.

Geological Society of America Special Papers 2006;403; 23-43
doi:10.1130/2006.2403(02)

Notes